
PROBABILISTIC LEARNING OF MULTIVARIATE TIME SERIES WITH TEMPORAL IRREGULARITY

A PREPRINT

Yijun LI

yijunli5-c@my.cityu.edu.hk

Cheuk Hang LEUNG

chleung87@cityu.edu.hk

Qi WU*

qi.wu@cityu.edu.hk

School of Data Science
City University of Hong Kong

June 19, 2023

ABSTRACT

Multivariate sequential data collected in practice often exhibit temporal irregularities, including nonuniform time intervals and component misalignment. However, if uneven spacing and asynchrony are endogenous characteristics of the data rather than a result of insufficient observation, the information content of these irregularities plays a defining role in characterizing the multivariate dependence structure. Existing approaches for probabilistic forecasting either overlook the resulting statistical heterogeneities, are susceptible to imputation biases, or impose parametric assumptions on the data distribution. This paper proposes an end-to-end solution that overcomes these limitations by allowing the observation arrival times to play the central role of model construction, which is at the core of temporal irregularities. To acknowledge temporal irregularities, we first enable unique hidden states for components so that the arrival times can dictate when, how, and which hidden states to update. We then develop a conditional flow representation to non-parametrically represent the data distribution, which is typically non-Gaussian, and supervise this representation by carefully factorizing the log-likelihood objective to select conditional information that facilitates capturing time variation and path dependency. The broad applicability and superiority of the proposed solution are confirmed by comparing it with existing approaches through ablation studies and testing on real-world datasets.

Keywords Robotics · Autonomous systems · Financial markets · Multivariate time series · Asynchronous data · Irregular sampling · Non-uniform time interval · Serial dependence · Multivariate dependence · Neural ODEs · Recurrent neural networks · Gated Recurrent Unit · Long short-term memory · Normalizing flow models · Conditional distribution · Joint distribution · Time-varying dynamics · Likelihood estimation · Probabilistic forecasting

*The corresponding author.

1 Introduction

Irregularly sampled time series are sequential recordings with unevenly spaced intervals between successive observation points. In the multivariate context, these time series can exhibit asynchrony because observations of individual component series may not align due to unevenly spaced intervals. These temporal irregularities arise whenever "missing" values occur in applications [1–3]. They could occur due to insufficient observation. For instance, in applications such as autonomous systems, tracking the position and speed of a group of moving objects often encounter missing values when certain objects travel behind obstacles or when the return signals attenuate differently. In this case, the observation process is constrained, hindering regular monitoring of continuously varying phenomena. They could also occur if observable events themselves arrive at inherently random times or with varying frequencies. For example, a liquid stock can trade on a regular trading day at a millisecond time scale. However, options contracts written on the same underlying stock may only trade once every few minutes. In this case, temporal irregularity is an intrinsic feature of the data-generating process. It is the liquidity disparity that results in the differences in time rather than a lack of observation.

Temporal irregularities, namely non-uniform time intervals, varying number of observations, and lack of alignment, pose challenges to the probabilistic forecasting of multivariate time series (MTS) data [4]. Probabilistic forecasting [5] involves specifying the target variables' joint distribution, learning its representation from data, and forecasting its time evolution. It is a fundamental task that includes the prediction problem of the mean, median, or specific quantile level as special cases. It also provides confidence intervals crucial for mission-critical downstream decision-making tasks [6]. However, the presence of temporal irregularities makes it challenging to model the distribution of MTS data, a defining characteristic of which is the existence of dependence structure [7].

At the component level, the dependence structure of MTS data is serial, meaning the marginal distributions of a given component variable conditional on different time points are not independent. In addition, different components can have different degrees and different natures of serial dependencies. Some exhibit short-ranged but nonlinear serial dependencies, while others are linear but long-ranged [7]. At the group level, the dependence structure refers to quantities such as the copula function of the joint distribution [8]. Specific components may depend more strongly on each other than on others. Moreover, both the component-level serial dependencies and the group-level inter-dependencies can vary over time; for instance, the autocorrelations of individual components and the copula function of the group data can be path dependent.

In other words, the distributional properties of MTS data can exhibit heterogeneities and vary over time, regardless of whether they are irregularly sampled. However, in cases where temporal irregularities are inherent to the data generation process, these irregularities reflect the underlying cause of these properties. Therefore, attributing them to missing values would be inappropriate. An ideal framework for probabilistic learning should acknowledge the intrinsic nature of uneven spacing and misalignments in the data and represent the associated data distribution accordingly. Before introducing our approach, we first review existing approaches to handling temporal irregularity and joint distribution modeling.

1.1 On Handling Temporal Irregularity

There are three primary approaches to handling irregular sampling. The first approach involves converting an irregularly sampled time series into one with evenly spaced time intervals before making predictions. The discretization method selects a larger uniformly spaced time interval, with each interval containing several observations, and computes the mean of these observations to represent the interval's value. However, this method loses local information due to averaging. In contrast, the imputation method interpolates the missing values of the lower-frequency components instead of averaging the higher-frequency components. It keeps the

local information of the higher-frequency components intact and uses models such as the Gaussian Process regression model [9], the Recurrent Neural Networks (RNNs) [10], and the Generative Adversarial Networks (GANs) [11] to impute the missing values of the lower-frequency components.

The next approach proposes using end-to-end models to avoid the "interpolate first and predict later" idea. This approach modifies classical recurrent architectures to encode the information embedded in irregular temporal patterns. For example, Che et al. [12] added an exponential decay mechanism in the hidden state. Neil et al. [13] extended the Long short-term memory (LSTM) unit by adding a new time gate controlled by a parametrized oscillation with a frequency range. Additionally, Mozer et al. [14] incorporated multiple time scales of the hidden state and made a context-dependent selection of time scales for information storage and retrieval. However, harnessing the uneven spacing property in the data and its asynchronous property is indirect using this approach and is less coherent compared to the Neural Ordinary Differential Equations (Neural ODEs) approach.

Chen et al. [15] introduced the Neural ODE framework by extending discrete neural networks into continuous-time networks, which makes it a natural candidate for handling data with arbitrarily small time intervals. For instance, De Brouwer et al. [16] embedded the Neural ODEs in the classical Gated Recurrent Unit (GRU) cell and derived the dynamics of the hidden state; Rubanova et al. [17] proposed the Latent ODE and were the first to embed Neural ODEs in a Variational Autoencoder to address the problem of irregularly sampled time series. Unlike the classical GRU cell, which keeps the hidden state constant in the absence of observations, the continuous-time GRU cell learns to evolve the hidden state using Neural ODEs. Building upon similar ideas, Lechner et al. [18] transformed the standard LSTM into a continuous version to address the issues of gradient vanishing and exploding. In section 2.1 and 2.2, we will provide more background on Neural ODEs and how to utilize them to model irregularly sampled data.

1.2 On Modeling Joint Data Distribution

For point estimation tasks, vanilla recurrent architectures, including RNN, GRU, and LSTM, can capture different aspects of the aforementioned properties of the MTS data. However, they are not directly applicable to distribution prediction due to the deterministic nature of the transition functions of their hidden states, which do not account for modeling uncertainties [19].

One class of models modifies the output function of neural networks to model the joint distribution or quantile function. For example, the models in [16, 20, 21] assume the data-generating process follows parametric distribution, such as the multivariate Gaussian (for continuous variables) and multivariate Negative Binomial (for discrete variables). To make the distribution time-varying, they condition the distribution parameters on hidden states and forecast them dynamically. Alternatively, researchers use quantile regression methods to fit the quantile function of the joint distribution. They use the quantile loss [22, 23] or the continuous ranked probability score (CRPS) [24] as the objective function to train the model and predict multiple quantile points simultaneously conditional on the hidden states.

Recently, unsupervised deep learning models have been utilized to learn the joint distribution of data, including combining Variational Autoencoders (VAEs) with RNNs [19] and integrating Normalizing Flows [25] into RNNs. Among these, two notable models are Real NVP (Real-valued Non-Volume Preserving) and MAF (Masked Autoregressive Flow). Real NVP defines a series of masked affine transformations, each of which splits the input data into two parts, applying a nonlinear transformation to one part while leaving the other unchanged. These invertible transformations facilitate both forward and inverse passes during training and generation. On the other hand, MAF is a normalizing flow model that employs autoregressive models to parameterize the inverse transformations. It transforms the input data through a series of invertible masked autoregressive layers, with each layer predicting the parameters of the conditional distribution for each

dimension based on the previously transformed dimensions. By conditioning on the previous dimensions, MAF captures complex dependencies in the data distribution.

The flow models are flexible in capturing intricate and evolving dependence structures and impose minimal assumptions about the functional form of the joint data distribution. These characteristics make them attractive for dealing with complex data, although they do not specifically address the structural aspects of irregular sampling. In section 2.3, we shall further detail the background of representing data distribution using the normalizing flow approach.

1.3 Our Approach and Contributions

Discussions in 1.1 and 1.2 unveil dislocations and disparities among ideas of handling temporal irregularities in the data and ideas to model its joint distribution. This paper bridges this gap by introducing a deep learning solution called the *Recurrent Flow Network* (RFN). It can seamlessly integrate the treatment of temporal irregularities with the learning of joint data distribution. Its novelties are as follows.

(i) The proposed RFN framework formulates a two-layer representation that distinguishes marginal learning of component dynamics from multivariate learning of joint data distribution. It is a versatile methodology that can be trained end-to-end and accommodate synchronous and asynchronous data structures. It also broadly applies to underlying recurrent architectures, including RNNs, GRUs, and LSTMs. Once the joint data distribution is learned, it is ready for sampling despite the distribution being non-parametrically represented via neural networks.

(ii) The marginal learning block addresses the component-level heterogeneity in the presence of unevenly spaced intervals. It achieves this by assigning unique sets of hidden states to individual variables, overcoming the drawback of disregarding statistical heterogeneities when hidden states are shared (e.g., in models like GRU-D [12], ODERNN [17], GRU-ODE-Bayes [16], and ODELSTM [18]), and by allowing the arrival times of component observations to determine how hidden states are updated, effectively avoiding data imputation.

(iii) The multivariate learning block then resolves the struggle faced by existing distribution models [16, 20, 21] in achieving a non-parametric representation of non-Gaussian data distribution, simultaneously with a flexible choice of information to generate time variation. The conditional CNF (Continuous Normalizing Flow) representation we develop enables one to choose what information to use to drive the time variation of the base distribution and the flow map without compromising any non-parametric capacity to represent the non-Gaussian data distribution.

(iv) Building upon (ii) and (iii), we strategically condition the log-likelihood objective on the observation times and along the component direction. This conditioning structure enables the optimizer to fully acknowledge and account for both the uneven spacing aspect and the asynchrony aspect of temporal irregularity in the MTS data. By conditioning on the observation times, the RFN ensures that the model incorporates the specific time points at which the data is observed. Additionally, conditioning along the component direction acknowledges the asynchrony between different variables, which arises exclusively in the multivariate context.

We validate the novelties mentioned above through three ablation studies using simulations and demonstrate the overall performance of the RFNs on three real-world datasets. The ablation studies simulate sample paths of a multivariate correlated Geometric Brownian Motion process to investigate the effects of sharing hidden states, imputing unobserved variables, and making different choices of conditional information. Meanwhile, the experimental datasets include the physical activities of the human body from the MuJoCo module [17], the climate records of weather from the USHCN dataset [26], and a three-year-long transaction record from HKEX comprising minute-level transactions for the stock with the largest market capitalization and its options. We compare four baseline models between their performance in vanilla forms and the performances utilizing

the RFN specification. The vanilla versions of these four baselines are GRU-D, ODERNN, GRU-ODE-Bayes, and ODELSTM. They are all designed to target multivariate irregularly sampled time series. The results show that the RFN framework has broad applicability and outperforms existing approaches significantly.

The rest of this paper is organized as follows. Section 2 provides the background knowledge that the RFNs build upon. Section 3 presents the data structure and necessary notations. Section 4 introduces model specifications for the marginal learning block. Sections 5 and 6 present methodologies of the multivariate learning block for the synchronous case and the asynchronous case. Section 7 discusses the ablation studies and the experiments. Finally, Section 8 concludes the paper. Additional formulations, proofs, extended numerics, and algorithms are provided in the Appendix A, B, C, and D respectively.

2 Backgrounds

Understanding the working mechanism of the proposed RFN model requires knowledge of Neural ODEs, their applications to model irregularly sampled data, and the flow representation of distributions. This section summarizes these subjects to make the paper self-contained. Throughout, we denote random variables as follows: X for scalar, \mathbf{X} for vector, and \mathbf{X} for matrix, and their corresponding sample values as x , \mathbf{x} , and \mathbf{x} , respectively.

2.1 Neural Ordinary Differential Equations

Neural ODEs were developed as the continuous limit of the ResNet model. The ResNet model solves the degradation problem of neural network [27–30] where researchers noticed that, as the network layers go deeper, the training loss begins to increase steadily once the network depth crosses a certain threshold. Consider a L -layer network, with x_0 being the input and x_l being the output of each layer $l \in \{1, \dots, L\}$. Instead of learning the mapping from x_0 to x_L directly, ResNet learns the difference between the input and output of each layer,

$$x_l = x_{l-1} + f_{\theta_l}(x_{l-1}). \quad (1)$$

The shortcut connections ensure that when adding one more layer, the worst scenario is that the learned residual is zero, resulting in the corresponding layer being an identity map. As a result, the training error will not increase when the model becomes deeper.

Chen et al. [15] proposed that taking the limit of the number of layers to infinity shall turn discrete layers into continuous layers. The resulting continuous limit of the recursive equation (1) is an ODE

$$\frac{dx(l)}{dl} = f_{\theta}(x(l), l). \quad (2)$$

Solving (2) with initial condition $x(0)$ is equivalent to the forward pass of ResNet. One can use numerical methods such as the Euler and the Runge–Kutta methods to solve (2). Similar to the role of backpropagation in discrete neural networks, the adjoint sensitivity method [31] computes gradients by solving an augmented ODE backward and updates parameters in continuous neural networks. The advantage of the adjoint sensitivity method is that it does not require storing intermediate quantities from the forward pass, enabling the training of Neural ODEs with constant memory.

2.2 Irregularly Sampled Time Series Modeling

Building on the insights from the Neural ODEs, researchers applied the continuous extension idea to model irregularly sampled MTS data using other recurrent architectures, such as ODERNN [17], GRU-ODE-Bayes [16], and ODELSTM [18]. For instance, De Brouwer et al. [16] derived the continuous-time dynamics of the

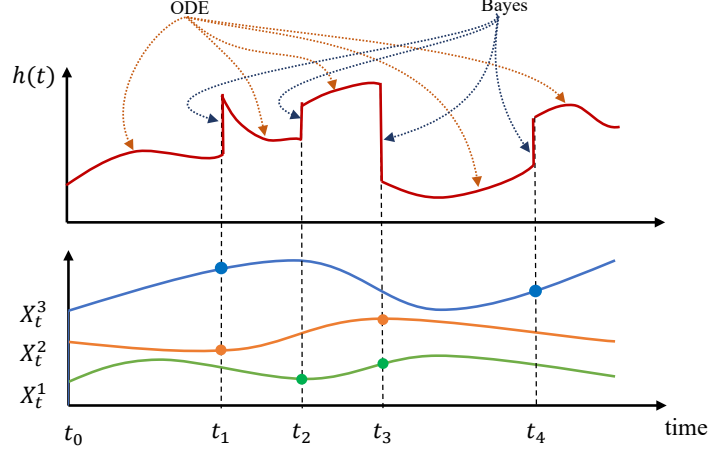


Figure 1: The evolution and update of hidden state in GRU-ODE-Bayes. Solid dots represent observed data points of X_t^1, X_t^2, X_t^3 . GRU-ODE evolves the hidden state in the absence of observations for all variables, while GRU-Bayes updates the hidden state when at least one variable has an observed value.

hidden states for the vanilla GRU cell and used ODE solvers to obtain its solution. The vanilla GRU has the following updating formulas

$$\begin{aligned}
 r_t &= \sigma(\mathbf{w}_r \mathbf{x}_t + \mathbf{u}_r \mathbf{h}_{t-1} + \mathbf{b}_r), \\
 z_t &= \sigma(\mathbf{w}_z \mathbf{x}_t + \mathbf{u}_z \mathbf{h}_{t-1} + \mathbf{b}_z), \\
 \tilde{\mathbf{h}}_t &= \tanh(\mathbf{w}_h \mathbf{x}_t + \mathbf{u}_h (r_t \odot \mathbf{h}_{t-1}) + \mathbf{b}_h), \\
 \mathbf{h}_t &= (1 - z_t) \odot \tilde{\mathbf{h}}_t + z_t \odot \mathbf{h}_{t-1},
 \end{aligned} \tag{3}$$

where $\mathbf{x}_t \in \mathbb{R}^D$ is the time- t MTS data; $r_t, z_t, \tilde{\mathbf{h}}_t, \mathbf{h}_t \in \mathbb{R}^H$ are vectors denoting the reset gates, the update gates, the candidate update gates, and the hidden states; $\mathbf{w}_{\{r,z,h\}} \in \mathbb{R}^{H \times D}$, $\mathbf{u}_{\{r,z,h\}} \in \mathbb{R}^{H \times H}$, and $\mathbf{b}_{\{r,z,h\}} \in \mathbb{R}^H$ are the matrix parameters to be trained; σ and \tanh are the sigmoid and the hyperbolic tangent activation function; the operator \odot denotes element-wise multiplication.

Subtracting \mathbf{h}_{t-1} on both sides of (3) leads to

$$\mathbf{h}_t - \mathbf{h}_{t-1} = (1 - z_t) \odot (\tilde{\mathbf{h}}_t - \mathbf{h}_{t-1}).$$

Then by taking the limit as the time difference between $t - 1$ and t tends to zero, one arrives at the continuous-time dynamics of the hidden states

$$\frac{d\mathbf{h}(t)}{dt} = (1 - \mathbf{z}(t)) \odot (\tilde{\mathbf{h}}(t) - \mathbf{h}(t)). \tag{4}$$

One can use (4) to evolve the hidden states during periods without observations and (3) to update the hidden state at observation time points. The continuous-time dynamics thus seamlessly interpolates hidden states between any two consecutive times of observations, accommodating unevenly spaced intervals. Figure 1 illustrates this process.

2.3 Unconditional Normalizing Flow

For tasks related to probabilistic forecasts, one needs a representation of the data distribution. Let $p(\mathbf{x})$, $\mathbf{x} \in \mathbb{R}^D$ be the probability density of the data-generating distribution and $p(\mathbf{z})$, $\mathbf{z} \in \mathbb{R}^D$ be the probability

density of the base distribution which is typically set as the standard normal, i.e., $Z \sim N(0, \mathbb{I}_D)$. The idea of the normalizing flow model is to find a differentiable bijective function f which can map samples from Z to X [32, 33]

$$f : \mathbb{R}^D \rightarrow \mathbb{R}^D; \quad f(z) = x.$$

In the discrete formulation, f is typically specified as a sequence of neural networks, $f = f_1 \circ \dots \circ f_{M-1} \circ f_M$. Given f and $p(z)$, one obtains $p(x)$ and $\log p(x)$ as

$$\begin{aligned} p(x) &= p(f^{-1}(x)) |\det[\partial_z f(z)]|^{-1}, \\ \log p(x) &= \log p(f^{-1}(x)) - \log |\det[\partial_z f(z)]|, \end{aligned}$$

via the change of variable formula, where $\det[\partial_z f(z)]$ is the determinant of the Jacobian matrix of f whose (i, j) entries are $\partial_{z_j} x_i$; $i, j = 1, \dots, D$.

However, designing the architectures of f_1, \dots, f_M is challenging because they need to satisfy three conditions: being bijective, differentiable, and facilitating the computation of the determinant of the Jacobian of the function f . Several models have thus been proposed, such as Real NVP [34], MAF [35], and GLOW [36]. See [37] for a complete introduction to the flow models.

The continuous normalizing flow model (CNF) [38] offers a solution to this challenge by extending the composition of discrete maps into a continuous map, whose differential form reads

$$\begin{aligned} \frac{\partial z(s)}{\partial s} &= f(z(s), s; \theta), s \in [s_0, s_1], \\ \text{where } z(s)|_{s=s_0} &= z, z(s)|_{s=s_1} = x. \end{aligned} \tag{5a}$$

Unlike the physical time t , s is called the *flow time* of the dynamics (5). At the initial flow time s_0 , the value of the flow $z(s_0)$ is set as z , which samples from the base distribution $p(z)$ of the base random variable Z . At the terminal flow time s_1 , the value of the flow $z(s_1)$ is set to equal x , which is the observed sample from the distribution of the true data-generating distribution $p(x)$.

The discrete formulation requires careful design of the weight matrices of f_j , $1 \leq j \leq M$ to be triangular to facilitate computing the Jacobian's determinant easily. The continuous formulation, however, replaces the computation of the Jacobian's determinant with relatively cheap trace operations, thanks to the Instantaneous Change of Variables theorem [15]. The log-density of the continuous flow therefore follows

$$\begin{aligned} \frac{\partial \log p(z(s))}{\partial s} &= -\text{Tr} [\partial_{z(s)} f], s \in [s_0, s_1], \\ \text{where } p(z(s))|_{s=s_0} &= p(z), p(z(s))|_{s=s_1} = p(x). \end{aligned} \tag{5b}$$

Solving equations (5a) and (5b) together, we have

$$\begin{bmatrix} x \\ \log p(x) \end{bmatrix} = \begin{bmatrix} z \\ \log p(z) \end{bmatrix} + \int_{s_0}^{s_1} \begin{bmatrix} f(z(s), s; \theta) \\ -\text{Tr} [\partial_{z(s)} f] \end{bmatrix} ds. \tag{5}$$

3 Data Structure

With enough background knowledge, we are ready to describe the data structure pertaining to the RFNs. Consider an MTS dataset containing N instances. Each instance is a D -dimensional sample path of the true data-generating process. All instances span the same $[0, T]$ period.

To account for the presence of temporal irregularity in a given instance $i \in \{1, \dots, N\}$, we first collect all time points at which at least one component series has an observation and define this collection as the time vector of observations,

$$\mathbf{t}^i := [t_1^i, \dots, t_{K_i}^i], \quad 0 \leq t_1^i \leq \dots \leq t_{K_i}^i \leq T.$$

For example, consider a simple dataset containing two univariate sample paths. The first sample path has four observations at physical time 1, 3, 5, 6 in units of seconds, and the second has three observations at 2, 4, 6. Then $K_1 = 4$ and $K_2 = 3$ with

$$\begin{aligned} \mathbf{t}^1 &= [t_1^1, \dots, t_{K_1}^1] = [t_1^1, t_2^1, t_3^1, t_4^1] = [1, 3, 5, 6], \\ \mathbf{t}^2 &= [t_1^2, \dots, t_{K_2}^2] = [t_1^2, t_2^2, t_3^2] = [2, 4, 6]. \end{aligned}$$

At a particular observation time $t \in \mathbf{t}^i$, we use $\mathbf{x}_{i,t} \in \mathbb{R}^{D \times 1}$ to denote the time- t sample values of the random vector \mathbf{X}_t in the i^{th} instance, within which we use $x_{i,t}^d \in \mathbb{R}$ to denote the d^{th} component, which is the sample value of the d^{th} random scalar X_t^d ,

$$\mathbf{x}_{i,t} := [x_{i,t}^1, \dots, x_{i,t}^d, \dots, x_{i,t}^D]', \quad t \in \mathbf{t}^i;$$

we then aggregate $\mathbf{x}_{i,t}$ from all observation times $t = t_1^i, t_2^i, \dots, t_{K_i}^i$ of the instance i to form the instance-level data matrix $\mathbf{x}_i \in \mathbb{R}^{D \times K_i}$,

$$\mathbf{x}_i := [\mathbf{x}_{i,t_1^i}; \mathbf{x}_{i,t_2^i}; \dots; \mathbf{x}_{i,t_{K_i}^i}]', \quad i \in [1, \dots, N];$$

finally, the entire MTS dataset is the collection of all N instances $\{\{\mathbf{x}_1\}; \{\mathbf{x}_2\}; \dots; \{\mathbf{x}_N\}\}$.

An instance \mathbf{x}_i can be synchronous or asynchronous depending on whether $x_{i,t}^d$ is observed or not for any combination of the variable dimension $d \in \{1, \dots, D\}$ and the observation time $t \in \mathbf{t}^i$.

Definition 1. Synchronous multivariate time series (Syn-MTS):

An instance \mathbf{x}_i where all of its D component series have observations at each and every time points $t \in \mathbf{t}^i$ (see Figure 2(a)).

Definition 2. Asynchronous multivariate time series (Asyn-MTS):

An instance \mathbf{x}_i where at least one of its D component series does not have all observations at all time point $t \in \mathbf{t}^i$ (see Figure 2(b)).

The following mask matrix \mathbf{m}_i makes the distinction between Asyn-MTS and Syn-MTS precise. For each instance i , given the data matrix \mathbf{x}_i , its mask matrix is defined as

$$\mathbf{m}_i := [m_{i,t_1^i}; m_{i,t_2^i}; \dots; m_{i,t_{K_i}^i}]',$$

where each vector $m_{i,t}$ denotes whether or not the constituent component variables are observed at time $t \in \mathbf{t}^i$,

$$\begin{aligned} m_{i,t} &:= [m_{i,t}^1, \dots, m_{i,t}^d, \dots, m_{i,t}^D]', \text{ where} \\ m_{i,t}^d &= \begin{cases} 1, & \text{if } x_{i,t}^d \text{ is observed;} \\ 0, & \text{if } x_{i,t}^d \text{ is unobserved.} \end{cases} \end{aligned}$$

In the sequel, we shall drop the instance script i to lighten notations, e.g., t_k^i , $\mathbf{x}_{i,t}$ and $m_{i,t}$ shall become t_k , \mathbf{x}_t and m_t , whenever the context is clear.

In the upcoming sections, we will see how this collection of data observation times permeates the marginal representation of individual variables, the formulation of cross-variable joint distribution, and the factorization of the log-likelihood, playing a pivotal role in coherently modeling the temporal irregularities at all stages.

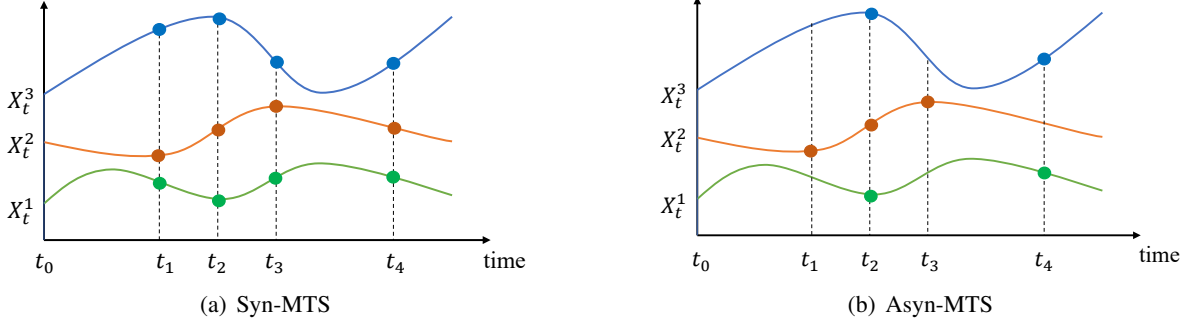


Figure 2: (a) and (b) are sample path examples of Syn-MTS and Asyn-MTS where observed data points are marked as solid circle dots. While the time intervals between consecutive observation times are unevenly spaced in both cases, component observations of the Syn-MTS sample path are always aligned. In contrast, in the Asyn-MTS case, no observation time has complete observations. This demonstrates that uneven spacing originates at the univariate level, while asynchrony arises exclusively in the multivariate context.

4 Marginal Learning

The marginal learning block aims to acknowledge heterogeneities and temporal irregularities in the component data by addressing two drawbacks of the hidden state-sharing feature in existing models. These drawbacks are present in vanilla recurrent architectures such as RNN, GRU, and LSTM, as well as models that build upon these vanilla recurrent architectures and target irregularly sampled time series such as those discussed in Section 1.1 and 2.2, i.e., ODERNN [17], GRU-ODE-Bayes [16], and ODELSTM [18].

Firstly, the statistical heterogeneities in the marginal dynamics may not be adequately captured when the hidden states are shared among component variables. The optimization process aims at minimizing the overall prediction error for all the variables. The shared hidden neurons are not optimized towards capturing the individual statistical features both statically, such as the maximum, the minimum, and the mean of each variable [39], and dynamically such as the range of serial dependencies [40].

Consider a multivariate financial series where one component variable is the stock price series, and the rest are the price series of its options at different strikes and maturities. The one-day price change of the APPLE stock, for example, is usually no more than a few percentages; however, the daily price swings of its options can be as wide as several times the base prices if strikes are far out of the money.

Secondly, when temporal irregularities are present, imputing unobserved variables introduces unnecessary biases if the hidden states are shared [41]. We illustrate this phenomenon in Figure 3. At time t_1 in the left figure, only $x_{t_1}^2$ has an observation while $x_{t_1}^1$ and $x_{t_1}^3$ are not observed. If we generate imputed values $\tilde{x}_{t_1}^1$ and $\tilde{x}_{t_1}^3$ and stack them together with the observed $x_{t_1}^2$, input data are biased by definition. The hidden state learned at t_1 will inherit these biases and carry them into the future due to its shared nature, even if all three components can be observed later such as t_2 . See the figure on the right.

Our solution is to assign unique sets of hidden states to component variables and let the arrival times of observations determine when, how, and which set of hidden states to update. This solution makes full use of the heterogeneous and asynchronous characteristics of the data but does not require imputing constituent variables in the absence of observations to complete the data. We use Figure 5 and the necessary formulation to demonstrate its working mechanism.

Figure 5(a) draws a synchronous sample path, and Figure 5(b) draws an asynchronous sample path. The sample paths are unevenly spaced in both cases, i.e., the lengths of time intervals (t_1, t_2) , (t_2, t_3) , and (t_3, t_4)

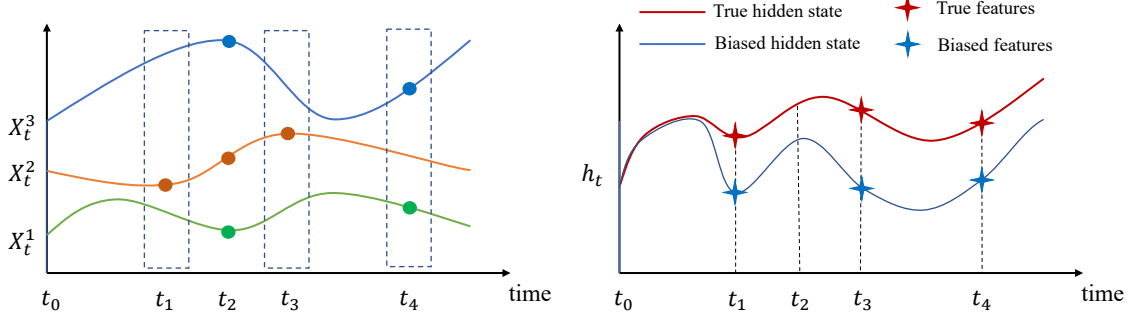


Figure 3: The left sub-figure draws a sample path of Asyn-MTS. A subset of variables have no observations at time t_1, t_3, t_4 ; The right sub-figure draws the corresponding shared hidden states. The learned hidden states are biased because the input data contain imputed, hence biased, values at time points t_1, t_3, t_4 .

are all different. However, data points in the synchronous case Figure 5(a) are aligned at all times t_1, t_2, t_3, t_4 . In contrast, no observation time has complete observations in the asynchronous case Figure 5(b). The following discussion is based on the asynchronous case. The synchronous case becomes a special case once the asynchronous case is clear.

Let the hidden states of the three component variables be h_t^1, h_t^2 , and h_t^3 . Recall that the vector $\mathbf{t} := [t_1, \dots, t_K]$ is the collection of all time points at which at least one component series has an observation. We specify equations governing the evolution of the hidden states in two regimes.

The *Continuous Updating* regime corresponds to continuous time intervals from t_{1+} to t_{2-} , t_{2+} to t_{3-} , t_{3+} to t_{4-} in Figure 5(b) when no component variables have observations. In this regime, we use equation (6) to evolve the marginal hidden states for all variables continuously. Here, t_- denotes the time point right before t and t_+ means the time point immediately after t .

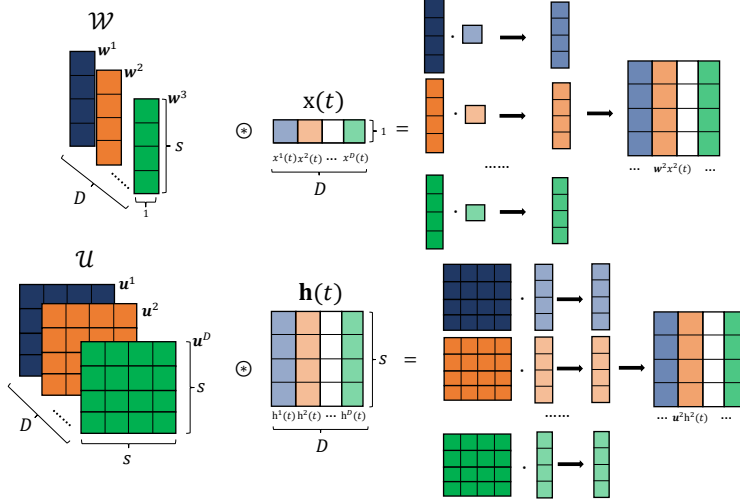
The *Discrete Updating* regime corresponds to the set of discrete time points $t = t_1, t_2, t_3, t_4$ at which at least one component variable is observed. In this case, we only update the marginal hidden states of those observed and keep the marginal hidden states of the unobserved variables unchanged per equation (7). For example, at t_1 , only $x_{t_1}^2$ and $x_{t_1}^3$, but not $x_{t_1}^1$, are observed. We therefore update $h_{t_1+}^2 = \text{GRU}^2(h_{t_1-}^2, x_{t_1}^2)$ and $h_{t_1+}^3 = \text{GRU}^3(h_{t_1-}^3, x_{t_1}^3)$, and leave $h_{t_1}^1$ unchanged, meaning $h_{t_1+}^1 = h_{t_1-}^1$.

In general, the continuous updating regulates the continuous no-observation periods $t \in [0, T] \setminus \mathbf{t}$ through Neural ODE (equation (6)), whereas the discrete updating governs the set of discrete times $t \in \mathbf{t}$ at which observations arrive via GRU (equation (7)). Together, they cover the entire evolution of the hidden states through time in $[0, T]$.

The complete formulation is as follows. For any $t \in [0, T]$, let $\mathbf{h}^d(t) \in \mathbb{R}^{S \times 1}$ be the d^{th} set of hidden states that is responsible for learning the d -th component variable, S be the dimension of each set of hidden states and $\mathbf{h}(t) \in \mathbb{R}^{S \times D}$ be the hidden states matrix of all components,

$$\mathbf{h}(t) = [\mathbf{h}^1(t); \dots; \mathbf{h}^d(t); \dots; \mathbf{h}^D(t)], t \in [0, T].$$

Correspondingly, the reset gates $\mathbf{r}^{\{c,u\}}(t)$, update gates $\mathbf{z}^{\{c,u\}}(t)$, and candidate update gates $\tilde{\mathbf{h}}^{\{c,u\}}(t)$ in both updating schemes, i.e. highlighted with the superscripts c and u , are all $\mathbb{R}^{S \times D}$ matrices.


 Figure 4: Schematic visualization of the two \otimes -related calculations in (8).

Continuous Updating:

$$\begin{aligned}
 & \forall t \in [0, T] \setminus \{t_1, \dots, t_K\}, \\
 & \frac{d\mathbf{h}(t)}{dt} = (1 - \mathbf{z}^c(t)) \odot (\tilde{\mathbf{h}}^c(t) - \mathbf{h}(t)), \text{ where} \\
 & \begin{cases} \mathbf{r}^c(t) = \sigma(\mathcal{W}_r^c \otimes \mathbf{x}(t) + \mathcal{U}_r^c \otimes \mathbf{h}(t) + \mathbf{b}_r^c), \\ \mathbf{z}^c(t) = \sigma(\mathcal{W}_z^c \otimes \mathbf{x}(t) + \mathcal{U}_z^c \otimes \mathbf{h}(t) + \mathbf{b}_z^c), \\ \tilde{\mathbf{h}}^c(t) = \tanh(\mathcal{W}_h^c \otimes \mathbf{x}(t) + \mathcal{U}_h^c \otimes (\mathbf{r}^c(t) \odot \mathbf{h}(t)) + \mathbf{b}_h^c). \end{cases}
 \end{aligned} \tag{6}$$

Discrete Updating:

$$\begin{aligned}
 & \forall t \in [t_1, \dots, t_K], \\
 & \mathbf{h}(t_+) := \mathbf{GRU}(\mathbf{h}(t_-), \mathbf{x}_t) \odot \mathbf{m}_t + \mathbf{h}(t_-) \odot (1 - \mathbf{m}_t), \\
 & \text{where } \mathbf{m}_t \in \mathbb{R}^{S \times D} \text{ and } \mathbf{GRU}(\mathbf{h}(t_-), \mathbf{x}_t) \in \mathbb{R}^{S \times D} \text{ are}
 \end{aligned} \tag{7}$$

$$\begin{cases} \mathbf{m}_t := [m_t^1; \dots; m_t^D]', \\ \mathbf{GRU}(\mathbf{h}(t_-), \mathbf{x}_t) := [\mathbf{GRU}^1(\mathbf{h}^1(t_-), x_t^1); \dots; \\ \mathbf{GRU}^d(\mathbf{h}^d(t_-), x_t^d); \dots; \mathbf{GRU}^D(\mathbf{h}^D(t_-), x_t^D)], \end{cases}$$

and the update formulas for **GRU** are

$$\begin{cases} \mathbf{r}^u(t_-) = \sigma(\mathcal{W}_r^u \otimes \mathbf{x}_t + \mathcal{U}_r^u \otimes \mathbf{h}(t_-) + \mathbf{b}_r^u), \\ \mathbf{z}^u(t_-) = \sigma(\mathcal{W}_z^u \otimes \mathbf{x}_t + \mathcal{U}_z^u \otimes \mathbf{h}(t_-) + \mathbf{b}_z^u), \\ \tilde{\mathbf{h}}^u(t_-) = \tanh(\mathcal{W}_h^u \otimes \mathbf{x}_t + \mathcal{U}_h^u \otimes (\mathbf{r}^u(t_-) \odot \mathbf{h}(t_-)) + \mathbf{b}_h^u), \\ \mathbf{h}(t_+) = (1 - \mathbf{z}^u(t_-)) \odot \tilde{\mathbf{h}}^u(t_-) + \mathbf{z}^u(t_-) \odot \mathbf{h}(t_-). \end{cases}$$

During the period from right after the k^{th} observation time to just before the next one, i.e., $[t_{k+}, t_{k+1-}]$, all component-wise hidden states $\mathbf{h}^d(t)$ evolve in the same fashion according to equation (6). However, when the physical time t passes through any of the observation times t_k , we check additionally which component

variables have observations and only update those using equation (7) via the standard GRUs,

$$\forall t \in [t_1, \dots, t_K], \forall d = 1, 2, \dots, D$$

$$\mathbf{h}^d(t_+) = \begin{cases} \text{GRU}^d(\mathbf{h}^d(t_-), x_t^d), & \text{if } m_t^d = 1; \\ \mathbf{h}^d(t_-), & \text{if } m_t^d = 0. \end{cases}$$

The set of parameters to be trained are

$$\zeta^{\{c,u\}} = \left\{ \mathcal{W}_{\{r,z,h\}}^{\{c,u\}}, \mathcal{U}_{\{r,z,h\}}^{\{c,u\}}, \mathbf{b}_{\{r,z,h\}}^{\{c,u\}} \right\},$$

where $\mathbf{b}_{\{r,z,h\}}^{\{c,u\}}$ are matrices in $\mathbb{R}^{S \times D}$. The parameters $\mathcal{W}_{\{r,z,h\}}^{\{c,u\}}$ and $\mathcal{U}_{\{r,z,h\}}^{\{c,u\}}$ are tensors in $\mathbb{R}^{D \times S \times 1}$ and $\mathbb{R}^{D \times S \times S}$ respectively

$$\mathcal{W} = \{\mathbf{w}^1; \dots; \mathbf{w}^D\}, \mathbf{w}^d \in \mathbb{R}^{S \times 1}$$

$$\mathcal{U} = \{\mathbf{u}^1; \dots; \mathbf{u}^D\}, \mathbf{u}^d \in \mathbb{R}^{S \times S}.$$

The operator \odot is the usual element-wise multiplication. The operator \otimes is defined as follows, resulting in $\mathbb{R}^{S \times D}$ matrices,

$$\mathcal{W} \otimes \mathbf{x}(t) := [\mathbf{w}^1 x^1(t); \dots; \mathbf{w}^D x^D(t)],$$

$$\mathcal{U} \otimes \mathbf{h}(t) := [\mathbf{u}^1 \mathbf{h}^1(t); \dots; \mathbf{u}^D \mathbf{h}^D(t)],$$
(8)

whose columns $\mathbf{w}^d x^d(t)$ and $\mathbf{u}^d \mathbf{h}^d(t)$ are in $\mathbb{R}^{S \times 1}$ for all $d \in \{1, \dots, D\}$.

Figure 4 visualizes the calculations in (8) schematically. Although each variable has distinct GRU parameters, there is no need to train them individually and separately, as it would be time-consuming and impractical for high-dimensional data. The tensor operations in (8), combined with the matrix formulations in (6-7), facilitate simultaneous training of all parameters together.

The formulations we provide so far use GRU and Neural ODE. However, the idea of using unique sets of hidden states and letting the arrival times of observations determine their updating is broadly applicable. We demonstrate its generality by providing formulations when the underlying is replaced by GRU-D, ODERNN, and ODELSTM in Appendix A.

5 Multivariate Synchronous Learning

Once the marginal learning block is set up, we seek to maximize the log-likelihood of all observations,

$$\max_{\Phi} \log p(\mathbf{x}_{t_1}, \dots, \mathbf{x}_{t_K}; \Phi),$$

where p is the joint density to be estimated from the observed data at all observation times $[t_1, \dots, t_K]$ and Φ is the parameter set.

5.1 Factorizing Log-likelihood Objective

If the multivariate sequence is synchronous, observing one variable implies the observation of all other component variables, despite potentially unevenly-spaced time intervals. Nevertheless, the synchronous

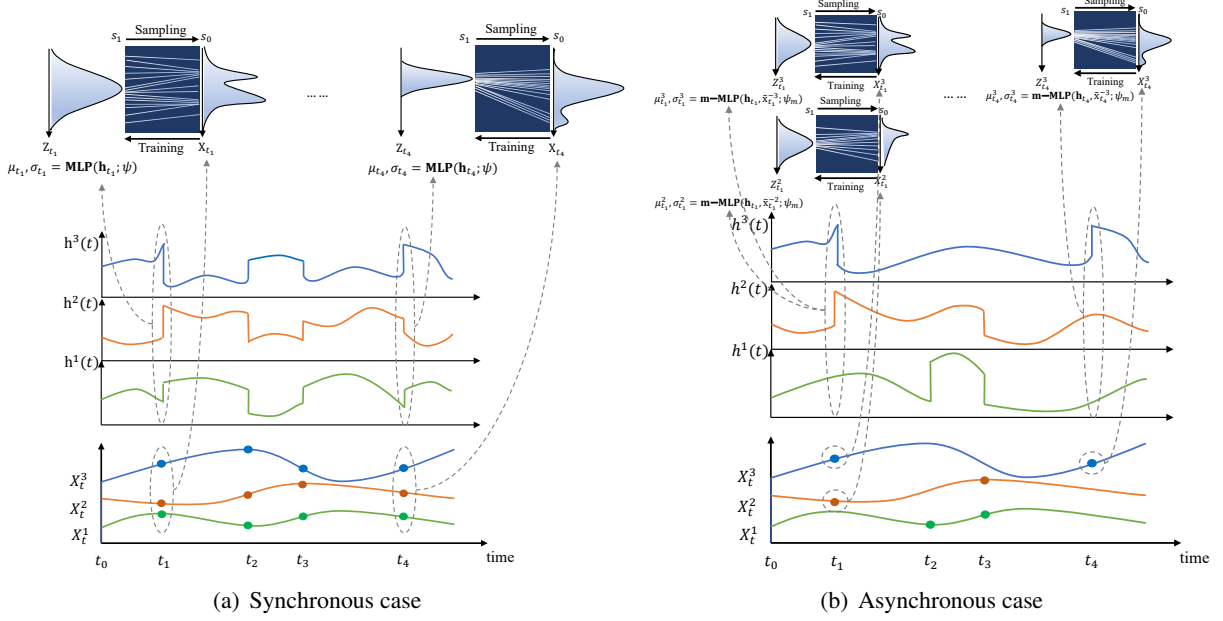


Figure 5: The framework of RFNs for (a) Syn-MTS and (b) Asyn-MTS. Both (a) and (b) have three component variables X_t^1, X_t^2, X_t^3 . The solid dots are observations. Different colors refer to different variables. In the marginal block, each variable has its own set of hidden states $h^1(t), h^2(t), h^3(t)$. The hidden states of a particular variable will be updated only when it has an observation. In the multivariate block, the time- t_k base distribution parameters, μ_{t_k} and Σ_{t_k} , are functions of the hidden states $\mathbf{h}_{t_{k-}} = [h_{t_{k-}}^1; h_{t_{k-}}^2; h_{t_{k-}}^3]$ for the Syn-MTS case and additionally the component variables $\mathbf{X}_{t_k}^{-d} := [x_{t_k}^1, \dots, x_{t_k}^{d-1}]$ for the Asyn-MTS case.

property ensures alignments, enabling the use of the chain rule of probability,

$$\begin{aligned}
 p(\mathbf{x}_{t_1}, \dots, \mathbf{x}_{t_K}; \Phi) &= p(\mathbf{x}_{t_1}; \phi_1) \cdot p(\mathbf{x}_{t_2} | \mathbf{x}_{t_1}; \phi_2) \cdot \dots \cdot p(\mathbf{x}_{t_K} | \mathbf{x}_{t_1}, \dots, \mathbf{x}_{t_{K-1}}; \phi_K) \\
 &= p(\mathbf{x}_{t_1}; \phi_1) \cdot \prod_{k=2}^K p(\mathbf{x}_{t_k} | \mathbf{x}_{t_1}, \dots, \mathbf{x}_{t_{k-1}}; \phi_k),
 \end{aligned} \tag{9}$$

which can be used to factorize the maximization of the joint log-likelihood at all observation times into optimizing conditional log-likelihoods individually,

$$\max_{\Phi} \log p(\mathbf{x}_{t_1}, \dots, \mathbf{x}_{t_K}; \Phi) = \max_{\phi_1} \log p(\mathbf{x}_{t_1}; \phi_1) + \sum_{k=2}^K \max_{\phi_k} \log p(\mathbf{x}_{t_k} | \mathbf{x}_{t_1}, \dots, \mathbf{x}_{t_{k-1}}; \phi_k),$$

where $\phi_k, k = 1, \dots, K$ is the parameter set of the conditional joint density at time t_k .

Note that the hidden states contain the exogenous information extracted from data. In particular, the amount of exogenous information carried by the historical observations up to t_{k-1} does not increase until the next observation arrives at t_k . Therefore, conditioning on the sample path $\mathbf{x}_{t_1}, \dots, \mathbf{x}_{t_{k-1}}$ can be faithfully approximated by conditioning on the hidden state at time t_{k-} ,

$$p(\mathbf{x}_{t_k} | \mathbf{x}_{t_1}, \dots, \mathbf{x}_{t_{k-1}}) \simeq p(\mathbf{x}_{t_k} | \mathbf{h}_{t_{k-}}),$$

under mild assumptions, except that the hidden states just before t_1 do not carry any exogenous data information as it is evolved from the initial hidden state \mathbf{h}_{t_0} by the Neural ODE. Thus, the time- t_1 conditional

density $p(\mathbf{x}_{t_1} | \mathbf{h}_{t_1-}; \phi_1)$ degenerates to its unconditional counterpart $p(\mathbf{x}_{t_1}; \phi_1)$. We can therefore maximize the hidden-states-conditioned log-likelihood $\log p(\mathbf{x}_{t_k} | \mathbf{h}_{t_k-}; \phi_k)$ instead,

$$\begin{aligned} \max_{\Phi} \log p(\mathbf{x}_{t_1}, \dots, \mathbf{x}_{t_K}; \Phi) &= \sum_{k=1}^K \max_{\phi_k} \log p(\mathbf{x}_{t_k} | \mathbf{x}_{t_1}, \dots, \mathbf{x}_{t_{k-1}}; \phi_k) \\ &\simeq \sum_{k=1}^K \max_{\phi_k} \log p(\mathbf{x}_{t_k} | \mathbf{h}_{t_k-}; \phi_k). \end{aligned} \quad (10)$$

5.2 Conditional Flow Representation

Optimizing (10) requires a conditional representation of the data distribution, wherein the log-densities can be tailored to suit one's specific conditional choices. For this purpose, we develop the following conditional formulation of the continuous normalizing flow.

Given two random variables X and Y , it represents the conditional log-density $\log p(x|y)$ of X through the non-parametric map f under the control of Y . We shall call this representation the Conditional CNF.

Lemma 1. *Let $\tilde{z}(s) = [z(s), y(s)]^T$ be a finite continuous random variable, and the probability density function of $\tilde{z}(s)$ is $p(\tilde{z}(s)) = p(z(s), y(s))$ which depends on flow time s , where $s_0 \leq s \leq s_1$. Given the governing dynamics of $\tilde{z}(s)$*

$$\begin{aligned} \frac{\partial \tilde{z}(s)}{\partial s} &= \begin{bmatrix} \frac{\partial z(s)}{\partial s} \\ \frac{\partial y(s)}{\partial s} \end{bmatrix} = \begin{bmatrix} f(z(s), s, y(s); \theta) \\ 0 \end{bmatrix}, \text{ where } s_0 \leq s \leq s_1, \\ z(s_1) &= x, \quad y(s_1) = y, \end{aligned}$$

and f is Lipschitz continuous in z and continuous in s for any y . We have

$$\log p(x, y) = \log p(z(s_0), y) - \int_{s_0}^{s_1} \text{Tr}[\partial_{z(s)} f(z(s), s, y; \theta)] ds. \quad (11)$$

Proof: See the Appendix B.

Proposition 5.1. *Let the assumptions in Lemma 1 hold. The conditional log-density $p(x|y)$ is given by*

$$\log p(x|y) = \log p(z(s_0)|y) - \int_{s_0}^{s_1} \text{Tr}[\partial_{z(s)} f(z(s), s, y; \theta)] ds. \quad (12)$$

Proof: Subtracting $\log p(y)$ on both sides of equation (11) in Lemma 1 and using the fact that $\log p(x, y) - \log p(y) = \log \frac{p(x, y)}{p(y)} = \log p(x|y)$ gives (12).

Proposition 5.1 overcomes the limitations of existing distribution models, which are either non-parametric² but static, such as models for images, or time-varying but parametric, such as models in [16, 20, 21] in which data distributions are assumed Gaussian path-dependent parameters. By extending the unconditional CNF formulation (see Section 2.3) to the conditional formulation, (12) allows the data distribution to be both non-parametric via the flow map f and time-varying, e.g., by choosing the conditional information y properly.

²By non-parametric, we meant the specific functional form of a distribution is not explicitly known. With this understanding, the data distribution represented by a neural network parameterized flow map is considered non-parametric despite neural nets being technically parameterized functions that are nonlinear.

5.3 Time-varying Specification

Our choice of the conditional information y is the hidden states. We shall let the hidden states determine the parameter values of the Gaussian base distribution. Because hidden states contain information of historical data and vary at different observation times, this choice of conditioning leads to path-dependent parameters of the base distribution. Consequently, upon transformation via the flow map, the data distribution also becomes path dependent.

Specifically, we use the standard Multilayer Perceptron (MLP) to map the time- t_{k-} hidden states $\mathbf{h}_{t_{k-}}$ learned from the marginal learning block to the mean vector μ_{t_k} and covariance matrix Σ_{t_k} of the Gaussian base

$$\begin{aligned} Z_{t_k} | \mathbf{h}_{t_{k-}} &\sim N(\mu_{t_k}, \Sigma_{t_k}), \text{ where} \\ \{\mu_{t_k}, \Sigma_{t_k}\} &= \mathbf{MLP}(\mathbf{h}_{t_{k-}}; \psi), \end{aligned} \quad (13)$$

resulting in the following conditional base density

$$p(\mathbf{z}_{t_k} | \mathbf{h}_{t_{k-}}; \mu_{t_k}, \Sigma_{t_k}) = \frac{\exp \left[-\frac{1}{2} (\mathbf{z}_{t_k} - \mu_{t_k})' \Sigma_{t_k}^{-1} (\mathbf{z}_{t_k} - \mu_{t_k}) \right]}{(2\pi)^{D/2} \det(\Sigma_{t_k})^{1/2}}.$$

This is in contrast with the unconditional flow models where the base distribution parameters are constants as it is a Standard Normal $Z \sim N(0, \mathbb{I}_D)$.

For example, at t_1 in Figure 5(a), the marginal hidden states $\{h_{t_1-}^1, h_{t_1-}^2, h_{t_1-}^3\}$ determine the t_1 Gaussian parameters $\{\mu_{t_1}, \Sigma_{t_1}\}$ of Z_{t_1} . The flow map f then transform samples from the Gaussian base density $p(\mathbf{z}_{t_1} | \mathbf{h}_{t_1-})$ non-parametrically and concurrently into t_1 samples of the data density $p(\mathbf{x}_{t_1} | \mathbf{h}_{t_1-})$.

It is worth noting that previous studies [16, 20, 21] also use hidden states to learn Gaussian parameters. However, those Gaussian parameters are associated with the data distribution. Our representation shifts the Gaussian assumption from the data distribution to the base distribution, and it is the base distribution parameters that depend on hidden states. This distinction is crucial because the resulting data distribution can now be non-parametric, non-Gaussian, and time-varying simultaneously.

Next, we use the following gated mechanism to incorporate the hidden state dependence into the flow map

$$f(\mathbf{z}(s), s, \mathbf{h}_{t_{k-}}; \theta) = (\mathbf{w}_z \mathbf{z}(s) + \mathbf{w}_h \mathbf{h}_{t_{k-}} + \mathbf{b}_z) \sigma(w_s s + b_s), \quad (14)$$

where $\mathbf{h}_{t_{k-}} \in \mathbb{R}^{H \times 1}$ is reshaped from the matrix $\mathbf{h}_{t_{k-}} \in \mathbb{R}^{S \times D}$ and σ is the sigmoid activation function. The set of trainable parameters θ includes $\mathbf{w}_h \in \mathbb{R}^{D \times H}$, $\mathbf{b}_z \in \mathbb{R}^D$, and $\{w_s, b_s\} \in \mathbb{R}$.

The first term $(\mathbf{w}_z \mathbf{z}(s) + \mathbf{w}_h \mathbf{h}_{t_{k-}} + \mathbf{b}_z)$ transforms the Gaussian samples from the base distribution to samples of the data-generating distribution subject to the influence of conditional information $\mathbf{h}_{t_{k-}}$. The second term $\sigma(w_s s + b_s)$ is the gate that modulates the magnitude multiplicatively of the first term through the *flow time* s . Together, they determine the instantaneous change of $\mathbf{z}(s)$

$$\begin{aligned} \frac{\partial \mathbf{z}(s)}{\partial s} &= f(\mathbf{z}(s), s, \mathbf{h}_{t_{k-}}; \theta), \quad s \in [s_0, s_1], \\ \text{where } \mathbf{z}(s)|_{s=s_0} &= \mathbf{z}_{t_k}, \quad \mathbf{z}(s)|_{s=s_1} = \mathbf{x}_{t_k}, \end{aligned}$$

where the initial value of the flow $\mathbf{z}(s)|_{s=s_0}$ is set as the Gaussian base sample \mathbf{z}_{t_k} , sampled from $Z_{t_k} | \mathbf{h}_{t_{k-}}$ per (13), and the terminal flow value $\mathbf{z}(s)|_{s=s_1}$ is set to equal the time- t_k observed data \mathbf{x}_{t_k} . Its solution, in integral form, maps samples from the base distribution to samples of the data distribution concurrently,

$$\mathbf{x}_{t_k} = \mathbf{z}_{t_k} + \int_{s_0}^{s_1} f(\mathbf{z}(s), s, \mathbf{h}_{t_{k-}}; \theta) ds, \quad (15)$$

Note that the mapping between \mathbf{z}_{t_k} and \mathbf{x}_{t_k} in (15) varies as the physical observation time t_k varies.

We summarize the time-varying specification of the conditional CNF representation for Syn-MTS data as follows. For $t_k \in [t_1, \dots, t_K]$,

$$\left[\log p(\mathbf{x}_{t_k} | \mathbf{h}_{t_{k-}}; \phi_{t_k}) \right] = \left[\log p(\mathbf{z}_{t_k} | \mathbf{h}_{t_{k-}}; \mu_{t_k}, \Sigma_{t_k}) \right] + \int_{s_0}^{s_1} \left[\begin{array}{c} \mathbf{f}(\mathbf{z}(s), s, \mathbf{h}_{t_{k-}}; \theta) \\ - \text{Tr}[\partial_{\mathbf{z}(s)} \mathbf{f}] \end{array} \right] ds. \quad (16)$$

It has two essential components, the time-varying base distribution driven by hidden states where ψ in (13) is the parameter to be trained, and the time-varying flow map indexed by observation arrival times with θ in (14) being the set of trainable parameters.

5.4 Training and Sampling

To train the FRN model, we maximize the conditional log-likelihoods (10) across all sample instances at all observation times. We set the dataset level log-likelihood $\mathcal{L}_{\text{Syn-MTS}}$ as the sample average of the N sample instances $\mathcal{L}_{\text{Syn-MTS}}^i$, $i = 1, \dots, N$, weighted by the number of observation times K_i of each instance,

$$\begin{aligned} \mathcal{L}_{\text{Syn-MTS}} &= \frac{1}{N} \sum_{i=1}^N \mathcal{L}_{\text{Syn-MTS}}^i \\ &= \frac{1}{N} \sum_{i=1}^N \frac{1}{K_i} \sum_{k=1}^{K_i} \log p(\mathbf{x}_{i,t_k} | \mathbf{h}_{i,t_{k-}}; \phi_{i,t_k}) \\ &= \frac{1}{N} \sum_{i=1}^N \frac{1}{K_i} \sum_{k=1}^{K_i} \left(\log p(\mathbf{z}_{i,t_k} | \mathbf{h}_{i,t_{k-}}; \mu_{i,t_k}, \Sigma_{i,t_k}) + \int_{s_1}^{s_0} \text{Tr} [\partial_{\mathbf{z}(s)} \mathbf{f}(\mathbf{z}(s), s, \mathbf{h}_{i,t_{k-}}; \theta)] ds \right). \end{aligned} \quad (17)$$

Once the model is trained, we can forecast the joint data distribution at time point t_k given the observations $\{\mathbf{x}_{t_1}, \dots, \mathbf{x}_{t_{k-1}}\}$ of the i^{th} instance. The confidence interval of predictions can be obtained by sampling from the learned joint distribution.

For sampling, we first obtain the hidden states $\mathbf{h}_{t_{k-}}$ for the i^{th} instance based on the observations $\{\mathbf{x}_{t_1}, \dots, \mathbf{x}_{t_{k-1}}\}$ per (6) and (7), and use $\mathbf{h}_{t_{k-}}$ to predict the base distribution parameters $\{\mu_{t_k}, \Sigma_{t_k}\}$ per (13). We then sample a given number of points \mathbf{z}_{t_k} from the base distribution with the predicted parameters. Finally, we transform these base sample points using the Conditional CNF map (15) to obtain concurrent samples that follow the data distribution.

6 Multivariate Asynchronous Learning

If the multivariate sequence is asynchronous, it implies the possibility that not all components of the vector \mathbf{x}_{t_k} are observable at any given time $t_k \in \mathfrak{t}$ (as defined in Definition 2). Note that the asynchrony aspect of temporal irregularities arises exclusively in the multivariate context, whereas the uneven spacing aspect originates essentially at the univariate level.

6.1 Additional Factorization of Log-likelihoods

To address the additional complication associated with asynchrony, we apply the chain rule of probability again to (9) along the component dimension to further factorize each conditional log-densities,

$$\begin{aligned} \log p(\mathbf{x}_{t_k} | \mathbf{h}_{t_{k-}}; \phi_k) &= \log \left(\prod_{d=1}^D p(x_{t_k}^d | \mathbf{h}_{t_{k-}}, x_{t_k}^1, \dots, x_{t_k}^{d-1}, \phi_{t_k}^d) \right) \\ &= \sum_{d=1}^D \log p(x_{t_k}^d | \mathbf{h}_{t_{k-}}, x_{t_k}^1, \dots, x_{t_k}^{d-1}, \phi_{t_k}^d), \end{aligned}$$

and define $\mathbf{x}_{t_k}^{-d}$ as follows to lighten the notation

$$\mathbf{x}_{t_k}^{-d} := [x_{t_k}^1, \dots, x_{t_k}^{d-1}]' \in \mathbb{R}^{(d-1) \times 1}$$

The maximization of the joint log-likelihood at all observation times then becomes

$$\begin{aligned} \max_{\Phi} \log p(\mathbf{x}_{t_1}, \dots, \mathbf{x}_{t_K}; \Phi) &= \sum_{k=1}^K \max_{\{\phi_k^1, \dots, \phi_k^D\}} \left(\log \prod_{d=1}^D p(x_{t_k}^d | \mathbf{h}_{t_{k-}}, \mathbf{x}_{t_k}^{-d}, \phi_{t_k}^d) \right) \\ &= \sum_{k=1}^K \max_{\{\phi_k^1, \dots, \phi_k^D\}} \left(\sum_{d=1}^D \log p(x_{t_k}^d | \mathbf{h}_{t_{k-}}, x_{t_k}^1, \dots, x_{t_k}^{d-1}, \phi_{t_k}^d) \right) \\ &= \sum_{k=1}^K \sum_{d=1}^D \max_{\phi_k^d} \log p(x_{t_k}^d | \mathbf{h}_{t_{k-}}, \mathbf{x}_{t_k}^{-d}, \phi_{t_k}^d). \end{aligned} \quad (18)$$

Factorization along the component dimension enables optimizing only the conditional distribution of variables with observations at a given observation point t_k , rather than optimizing for all D variables.

Note that different from the Syn-MTS case (equation (10)), the conditional information in (18) contains not only the historical information embedded in the hidden states $\mathbf{h}_{t_{k-}}$, but also the concurrent information from the cross-variables $\mathbf{x}_{t_k}^{-d}$ at t_k . Below we show how to embed the concurrent information into the base distribution and the flow map.

6.2 Conditional Information Specification

Firstly, for the base distribution, unlike the Syn-MTS case that uses the standard fully-connected MLP to map hidden states $\mathbf{h}_{t_{k-}}$ to the distribution parameters μ_{t_k} and Σ_{t_k} , we shall design a masked-MLP (**m-MLP**) that keeps only the first $d-1$ variables $[x_{t_k}^1, \dots, x_{t_k}^{d-1}]$ by muting the rest $[x_{t_k}^{d+1}, \dots, x_{t_k}^D]$,

$$\{\mu_{t_k}^d, \Sigma_{t_k}^d\} = \mathbf{m}\text{-MLP}(\mathbf{h}_{t_{k-}}, \mathbf{x}_{t_k}^{-d}; \psi_m), \quad (19)$$

where $\mu_{t_k}^d \in \mathbb{R}^1$ and $\Sigma_{t_k}^d \in \mathbb{R}^{1 \times 1}$. Figure 6 draws the architecture of the masked-MLP, where the inputs are the hidden states and all variables, and the outputs are the parameters of the base distribution with different conditioned information.

Secondly, for the flow model, we reshape the hidden state matrix $\mathbf{h}_{t_{k-}} \in \mathbb{R}^{S \times D}$ into vector $\mathbf{h}_{t_{k-}} \in \mathbb{R}^{H \times 1}$, and encode it into flow model, similar to treatment in the Syn-MTS case. In addition, in Asyn-MTS, we also need to fuse concurrent variables $\mathbf{x}_{t_k}^{-d}$ into the flow map,

$$\mathbf{f}(z^d(s), s, \mathbf{h}_{t_{k-}}, \mathbf{x}_{t_k}^{-d}; \theta) = (w_z z^d(s) + w_h \mathbf{h}_{t_{k-}} + w_x \mathbf{x}_{t_k}^{-d} + b_z) \sigma(w_s s + b_s), \quad (20)$$

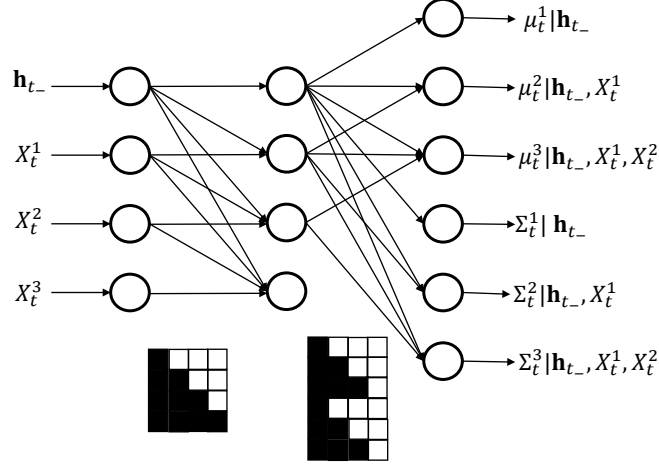


Figure 6: The architecture of the masked-MLP (**m-MLP**). The Bottom two squares are weight matrices for the first layer and second layer, in which the shaded squares represent the trainable parameters and the unshaded squares represent the parameters set to zero in the training process.

where $\{w_z, b_z, w_s, b_s\} \in \mathbb{R}$, $w_x \in \mathbb{R}^{1 \times (d-1)}$, $w_h \in \mathbb{R}^{1 \times H}$ are trainable parameters.

Note that the observation time t_k is defined as a time whenever constituent variables have observations. It does not guarantee every constituent variable has full observations. In this case, we use the marginal predictions

$$\begin{aligned} \tilde{x}_{t_k} &= x_{t_k} \odot m_{t_k} + \hat{x}_{t_k} \odot (1 - m_{t_k}) \\ \text{where } \hat{x}_{t_k} &= g(\mathbf{h}_{t_{k-}}; \eta), \end{aligned}$$

to address the issue that certain variables in the vector $x_{t_k}^{-d}$ are still "missing" even if we only optimize the conditional distribution of the observed variables at this time. Here $g : \mathbb{R}^{S \times D} \rightarrow \mathbb{R}^D$ is a function that maps the hidden states to values in data series, with η being the trainable parameter. Equation (18) therefore becomes

$$\max_{\Phi} \log p(x_{t_1}, \dots, x_{t_K}; \Phi) = \sum_{k=1}^K \sum_{d=1}^D \max_{\phi_t^d} \log p(x_{t_k}^d | \mathbf{h}_{t_{k-}}, \tilde{x}_{t_k}^{-d}; \phi_{t_k}^d), \quad (21)$$

where $\tilde{x}_{t_k}^{-d} := [\tilde{x}_{t_k}^1, \dots, \tilde{x}_{t_k}^{d-1}]'$.

We summarize the conditional CNF representation for Asyn-MTS data as

$$\left[\log p(x_{t_k}^d | \mathbf{h}_{t_{k-}}, \tilde{x}_{t_k}^{-d}; \phi_{t_k}^d) \right] = \left[\log p(z_{t_k}^d | \mathbf{h}_{t_{k-}}, \tilde{x}_{t_k}^{-d}; \mu_{t_k}^d, \Sigma_{t_k}^d) \right] + \int_{s_0}^{s_1} \left[f(z^d(s), s, \mathbf{h}_{t_{k-}}, \tilde{x}_{t_k}^{-d}; \theta) - \text{Tr} [\partial_{z^d(s)} f] \right] ds \quad (22)$$

where the scalar sample $z_{t_k}^d$ is a realization of

$$Z_{t_k}^d | \mathbf{h}_{t_{k-}}, \tilde{x}_{t_k}^{-d} \sim N(\mu_{t_k}^d, \Sigma_{t_k}^d),$$

whose parameters ψ_m are learned through (19).

6.3 Training

There are two tasks in training the Asyn-MTS model, maximizing the log-likelihood of observations and imputing the missing values accurately. Therefore, different from the objective function (equation (18)) of

the Syn-MTS model, we add the Mean Square Error (MSE) term to the objective function of the Asyn-MTS model,

$$\mathcal{L}_{\text{Asyn-MTS}}^i = \sum_{k=1}^{K_i} \sum_{d=1}^D \frac{1}{K_i D} \left[(x_{i,t_k}^d - \hat{x}_{i,t_k}^d)^2 \odot m_{i,t_k}^d + \log p(z_{i,t_k}^d | \mathbf{h}_{i,t_{k-}}^d, \tilde{\mathbf{x}}_{i,t_k}^{-d}; \mu_{i,t_k}^d, \Sigma_{i,t_k}^d) + \int_{s_1}^{s_0} \text{Tr}[\partial_{z^d(s)} \mathbf{f}] ds \right]. \quad (23)$$

Here, we only compute the MSE associated with the variables that have observations since we have no ground truth of the unobserved one. The dataset level log-likelihood is then the sum of $\mathcal{L}_{\text{Asyn-MTS}}^i$ for all sample instances.

6.4 Sampling

The sampling process at time t_k of the Asyn-MTS model differs from that of the Syn-MTS model and is similar to the Gibbs sampling. We first predict the parameters of base distribution of variable $X_{t_k}^1$ conditional on the hidden state $\mathbf{h}_{t_{k-}}$ from marginal learning block, i.e., $\{\mu_{t_k}^1, \Sigma_{t_k}^1\} = \mathbf{m}\text{-MLP}(\mathbf{h}_{t_{k-}}; \psi_m)$. Then, we sample a given number of points $z_{t_k}^1$ from this base distribution, and we transform these points using the flow model. Next, we predict the parameters of base distribution of variable $X_{t_k}^2$ conditional on the hidden state $\mathbf{h}_{t_{k-}}$ and the generated samples of $X_{t_k}^1$, i.e., $\{\mu_{t_k}^2, \Sigma_{t_k}^2\} = \mathbf{m}\text{-MLP}(\mathbf{h}_{t_{k-}}, x_{t_k}^1; \psi_m)$. Then, we obtain samples $z_{t_k}^2$ from the second base distribution and transform these points using the flow model. The process continues until the last variable is sampled.

We verify the components proposed above by further ablation studies in section 7.3. The algorithms for the training and sampling procedures of the Syn-MTS model and the Asyn-MTS model are provided in Appendix D.

7 Experiments

We conduct three ablation studies to assess the efficacy of the model specification, followed by three experiments using real-world datasets to evaluate the overall performance of the RFNs. In all studies and experiments, we use 70% of the sample instances for training, 15% for validation, and 15% for testing.

All studies and experiments are run on Dell Precision 7920 Workstations with Intel(R) Xeon(R) Gold 6256 CPU at 3.60GHz, and three sets of NVIDIA Quadro GV100 GPUs. All models are implemented in Python 3.8. The versions of the main packages of our code are: Pytorch 1.8.1+cu102, torchdiffq: 0.2.2, Sklearn: 0.23.2, Numpy: 1.19.2, Pandas: 1.1.3, Matplotlib: 3.3.2.

7.1 Baseline Models

We set up four baseline models, GRU-D, ODERNN, GRUODE, and ODELSTM, with and without an RFN specification. In their vanilla forms, these baselines all aim to model multivariate irregularly sampled time series but assume observations follow a multivariate normal distribution and predict parameters of the data distribution based on the hidden state. To compare the vanilla form of a baseline model, e.g., GRU-D, with its RFN counterpart, e.g., termed as RFN-GRU-D, we use the corresponding RFN specifications laid out in Appendix A as the marginal learning block, for instance, (A.1) for GRU-D, (A.2) for ODERNN, (A.3) for ODELSTM, and use the formulations in Section 5 and 6 for the multivariate learning. For GRUODE, its RFN specification has been discussed in length in the main body of the paper (see (6) and (7)). Hyperparameters, such as learning rate and batch size, are tuned using a random search for all experiments. The 'dopri5' method

is employed as the numerical solver for the ODE-based models. The parameters of the best model obtained during training are saved for testing purposes.

7.2 Evaluation Metric

We use the Continuous Ranked Probability Score (CRPS) [42] as the evaluation metric to measure the proximity between the learned distribution and the empirical distribution of data. The CRPS metric is the suitable scoring function for the evaluation since it attains the minimum when the learned distribution of data aligns with its empirical distribution. The CRPS is defined as

$$\text{CRPS}(\hat{F}, x) = \int_{\mathbb{R}} (\hat{F}(z) - \mathbb{I}\{x \leq z\})^2 dz,$$

where \hat{F} is the estimated CDF of random variable X and x is the realized observations of X . In our dataset, the observations are irregularly sampled, and some values are missing, and thus we only compute CRPS when the variables can be observed.

Since CRPS targets to evaluate the estimated distribution of the univariate random variable, [21] suggests using CRPS_{sum} as a new proper multivariate-scoring rule to evaluate the estimated distribution of multivariate random variables,

$$\text{CRPS}_{\text{sum}} = \mathbb{E}_t \left[\text{CRPS} \left(\hat{F}_{\text{sum}}(t), \sum_{d=1}^D x_t^d \right) \right],$$

where \hat{F}_{sum} is computed by adding the estimated CDF of all variables together. In practice, the empirical CDF is always used to represent \hat{F} and \hat{F}_{sum} . In our experiments, we take 100 samples from trained models to estimate the empirical CDF. For Asyn-MTS datasets, some variables are not observable at an observation time; we thus only add the estimated CDF of observed variables as \hat{F}_{sum} .

7.3 Ablation Studies via Simulation

(a) Data Generating Process. We set the Data Generation Process (DGP) $X_t = [X_t^1, \dots, X_t^5]$ as the following continuous-time correlated Geometric Brownian Motion (GBM) [43] to generate sample instances,

$$dX_t = \mu \odot X_t dt + \text{diag}(\sigma \odot X_t) dW_t, \quad t \geq 0, \quad (24)$$

where $\mu = [\mu^1, \dots, \mu^5]'$ and $\sigma = [\sigma^1, \dots, \sigma^5]'$ are the drift term and volatility term of variables, and $W_t = [W_t^1, \dots, W_t^5]'$ is the multivariate Brownian Motion process such that $\langle dW_t^i, dW_t^j \rangle = \rho_{ij}(t) dt$ where

$$[\rho_{ij}(t)]_{1 \leq i, j \leq 5} := \sin \left(\frac{\pi}{2} t \right) \begin{bmatrix} 1 & \rho_1 & 0 & 0 & 0 \\ \rho_1 & 1 & 0 & 0 & 0 \\ 0 & 0 & 1 & \rho_2 & \rho_2 \\ 0 & 0 & \rho_2 & 1 & \rho_2 \\ 0 & 0 & \rho_2 & \rho_2 & 1 \end{bmatrix}.$$

We devise such a correlated GBM as the DGP for several reasons. Firstly, the GBM is a continuous-time stochastic process where the instantaneous changes of state variables are explicitly governed by stochastic differential equations (SDEs). It is a fundamental model in describing diffusive phenomena in physics and random fluctuations of asset prices in financial markets, for example, in the Black-Scholes model [44]. Secondly, the correlated GBM admits log-normal distribution for each variable, distinguishing it from the

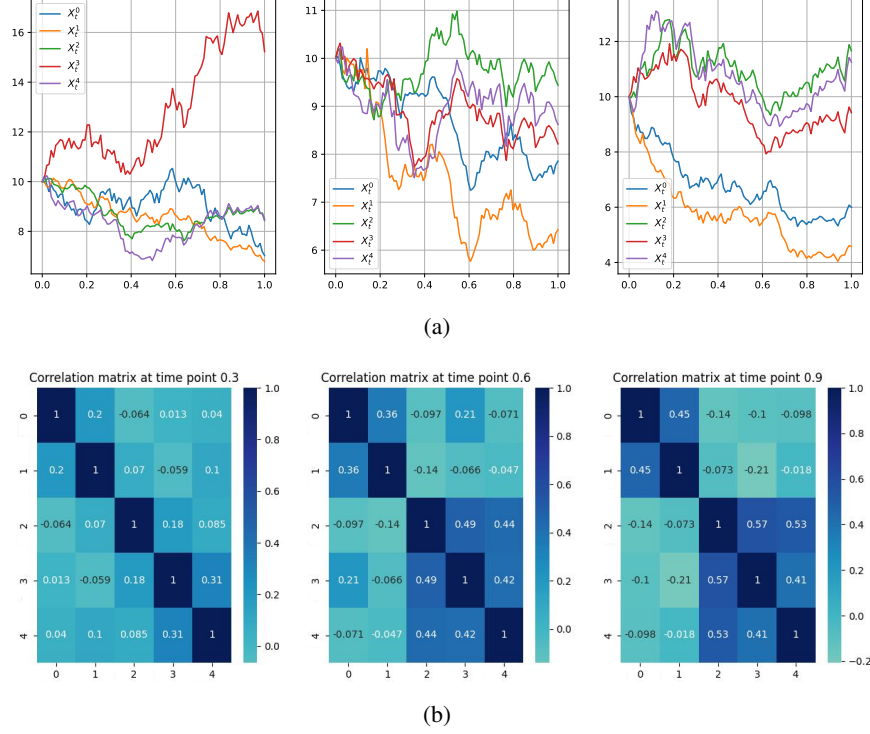


Figure 7: (a) Three representative sample paths. (b) The sample correlation matrix at observed time points 0.3, 0.6, 0.9.

normal distribution. The flexibility in setting the drift, volatility, and correlation terms allows one to generate diverse statistical properties of the sample paths. Thirdly, the correlation among the five variables is not set to static but time-varying, gradually increasing as time progresses from 0 to 1 due to the sinusoidal function $\sin(\frac{\pi}{2}t)$. This guarantees that the joint distribution of the five variables is constantly changing. Figure 7(a) showcases three representative sample paths from the dataset. Additionally, Figure 7(b) illustrates the sample correlation matrix at observed time points 0.3, 0.6, and 0.9, validating the dynamic and gradual increase in correlation.

(b) Simulation Settings. We first simulate 1,000 sample paths using (24) with uniform time intervals. The Brownian parameters, i.e., the drift terms and the diffusion terms, of the 1,000 sample paths are set as

$$\begin{aligned}
 \mu^1 &= \mu^2 \sim \text{Unif}(-0.2, -0.05), \\
 \mu^3 &= \mu^4 = \mu^5 \sim \text{Unif}(0.05, 0.2), \\
 \sigma^1 &= \sigma^2 \sim \text{Unif}(0.15, 0.3), \\
 \sigma^3 &= \sigma^4 = \sigma^5 \sim \text{Unif}(0.15, 0.3),
 \end{aligned}$$

where $\text{Unif}(\cdot, \cdot)$ stands for a uniform distribution.

We create the Syn-MTS and Asyn-MTS datasets through random sampling from the simulated dataset with complete observation. In the Syn-MTS dataset, we randomly choose half of the time points and sample the corresponding observations X_t at the chosen time points. To generate the Asyn-MTS dataset, we randomly eliminate half of the observations for each variable. The elimination is independent between any two variables. Therefore, some variables have observations at an observed time point, and some variables do not.

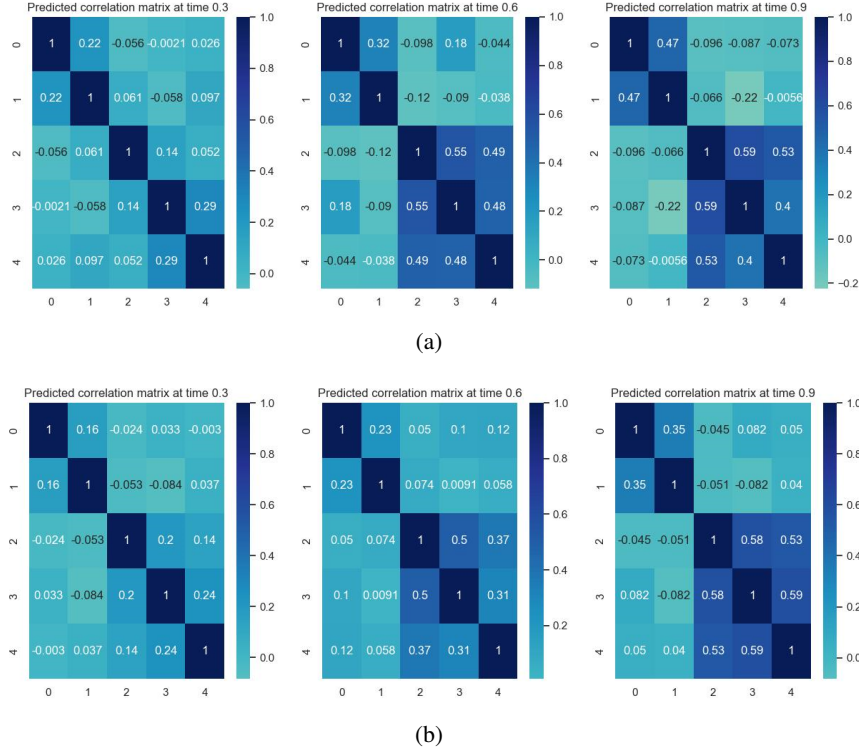


Figure 8: The sample correlation matrix recovered from the learned Syn-MTS model (a) and the learned Asyn-MTS model (b) at 0.3, 0.6, and 0.9.

Table 1: **Geometric Brownian Motions:** Baseline models in vanilla form (column 2,3) vs. using RFN specification (column 5,6). Numbers underneath CRPS, CRPS_{sum} are displayed in the form of mean \pm std, averaged over five experiments. The last two columns CRPS \uparrow and CRPS_{sum} \uparrow report percentage increases of performance using RFN specification.

model	CRPS	CRPS _{sum}	model	CRPS	CRPS _{sum}	CRPS \uparrow	CRPS _{sum} \uparrow
<i>Syn-MTS</i>							
GRUODE	0.2428 \pm 0.0135	0.9423 \pm 0.0831	RFN-GRUODE	0.1947 \pm 0.0048	0.6116 \pm 0.0255	19.83%	35.01%
ODELSTM	0.2556 \pm 0.0101	1.0219 \pm 0.0456	RFN-ODELSTM	0.1914 \pm 0.0044	0.5946 \pm 0.0062	25.12%	41.81%
GRU-D	0.2227 \pm 0.0148	0.8253 \pm 0.0948	RFN-GRU-D	0.1903 \pm 0.0029	0.5922 \pm 0.0059	14.54%	28.24%
ODERNN	0.2543 \pm 0.0230	1.0025 \pm 0.1439	RFN-ODERNN	0.1940 \pm 0.0012	0.6077 \pm 0.0074	23.72%	39.38%
<i>Asyn-MTS</i>							
GRUODE	0.2475 \pm 0.0061	0.4982 \pm 0.0172	RFN-GRUODE	0.1884 \pm 0.0020	0.3410 \pm 0.0039	23.90%	31.54%
ODELSTM	0.3164 \pm 0.0639	0.6185 \pm 0.1106	RFN-ODELSTM	0.1927 \pm 0.0028	0.3472 \pm 0.0021	39.09%	43.86%
GRU-D	0.2344 \pm 0.0049	0.4670 \pm 0.0105	RFN-GRU-D	0.1902 \pm 0.0016	0.3506 \pm 0.0054	18.87%	24.92%
ODERNN	0.2315 \pm 0.0057	0.4597 \pm 0.0105	RFN-ODERNN	0.1909 \pm 0.0021	0.3446 \pm 0.0045	17.56%	25.04%

(c) Data and Model Validation. The experiment results in Table 1 demonstrate that RFNs (e.g., RFN-GRUODE, RFN-ODELSTM, RFN-GRU-D, RFN-ODERNN) outperform the corresponding baselines with smaller CRPS and CRPS_{sum}. This indicates the superior ability of the RFNs to capture the joint distribution of multivariate irregularly sampled time series at each observed time point and recover its dynamics. Figure 8(a) and 8(b) illustrate the correlation matrices sampled from the estimated Syn-MTS and Asyn-MTS models at observed time points 0.3, 0.6, and 0.9, closely resembling the ground truth in Figure 7(b). The correlation coefficients from the recovered matrices gradually transition from weak to strong as time progresses, aligning

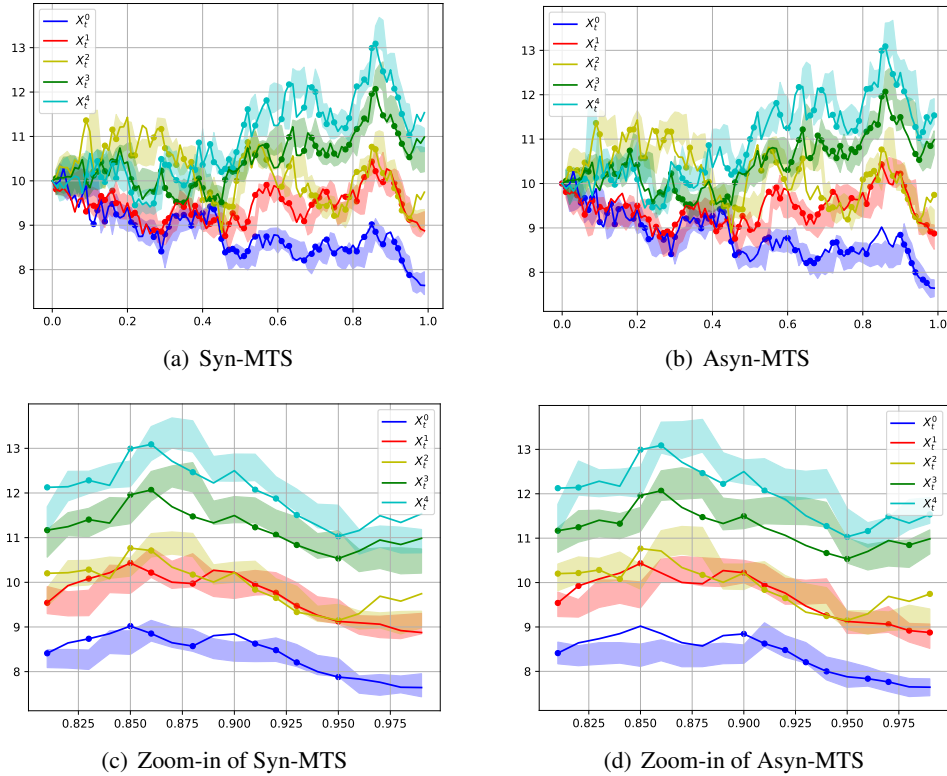


Figure 9: Predicted quantile intervals (shaded area) from 20% to 80% of Syn-MTS data (a,c) and Asyn-MTS data (b,d) using the RFN-GRUODE specification. Solid dots represent observations. Broader quantile ranges are available in Appendix C.

with the ground truth in Figure 7(b). This dynamic capture of the joint distribution validates the effectiveness of the RFN specification. Lastly, we employ the RFNs for interval estimation of correlated GBM processes. Figure 9(a) and Figure 9(b) display prediction intervals for Syn-MTS and Asyn-MTS, respectively, while Figure 9(c) and Figure 9(d) provide a closer view of the predicted Syn-MTS and Asyn-MTS.

(d) Effects of Sharing Hidden States. We first examine the proposition that training each component variable independently in the marginal learning block can mitigate the biases introduced by sharing hidden states, therefore better capturing component heterogeneities.

The comparison is between training an RFN model using one shared set of hidden states in the marginal learning block versus assigning unique sets of hidden states to variables. Results from Figure 10 and 11 indicate that training variables independently yield consistent and noticeable positive improvements in the Syn-MTS model. Since the data is synchronous, component variables differ only in their statistical features, statically and dynamically. This shows the importance of preserving heterogeneities in the marginal distributions and their dynamics. Meanwhile, the improvements become much more significant when data is asynchronous, implying that the biases caused by and spread from sharing hidden states among variables (see Figure 3 for an illustration) are almost unbearable.

(e) Effects of Imputing Unobserved Variables. When we specify the multivariate asynchronous learning block in Section 6, we posit that there are two ways to handle concurrent "missing" values across variables at a given observation time.

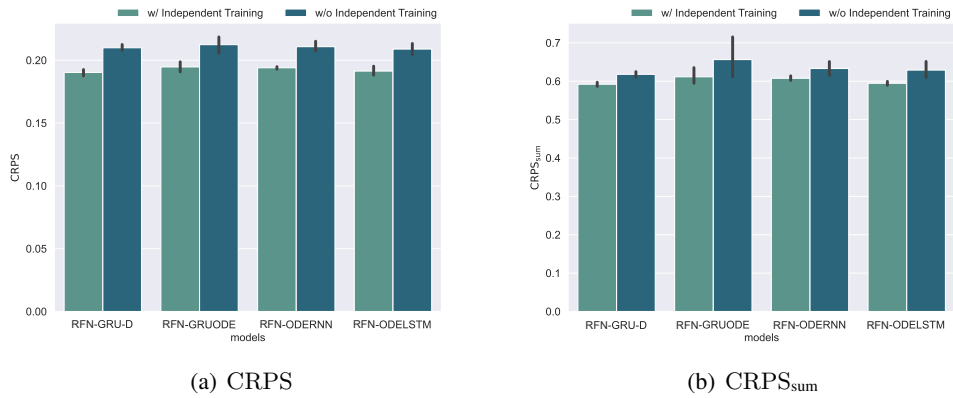


Figure 10: Syn-MTS: Training variables independently (left bars in lighter green) vs. Sharing hidden states (right bars in darker green). The smaller the values of CRPS and CRPS_{sum} are, the better.

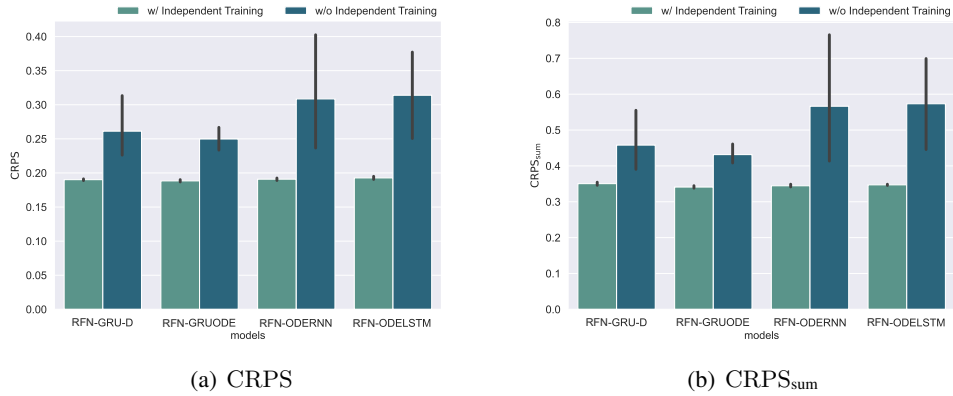


Figure 11: Asyn-MTS: Training variables independently (left bars in lighter green) vs. Sharing hidden states (right bars in darker green).

We can either impute the unobserved variables, which completes the asynchronous dataset into a synchronous one and train them using the Syn-MTS model, or utilize our Asyn-MTS model, where we factorize the conditional log-likelihood along the component dimension one more time at any observation time, and only compute the resulting factorized conditional log-likelihoods for variables that have observations. In other words, the objective function (18) avoids computing any loss terms for unobserved variables. The unobserved variables only serve as concurrent conditional information for computing the conditional likelihoods of observed variables. Figure 12 indicates clearly that our approach (the left bars in lighter green), without completing the data, is indeed robustly superior than the "imputing before training" approach, where the unobserved variables are imputed by their marginal block forecasts, despite it being more intuitive.

(f) Effects of Conditional Choices. Third, in the Asyn-MTS model, we model the distribution of observed variables conditional on the historical information via hidden states \mathbf{h}_{t_k} and the concurrent information $\tilde{\mathbf{x}}_{t_k}^{-d}$, i.e., $\log p(\mathbf{x}_{t_k}^d | \mathbf{h}_{t_k}, \tilde{\mathbf{x}}_{t_k}^{-d})$ in equation (21). We conduct an ablation study that computes the distribution only conditional on the past values and drops the concurrent values, i.e., $\log p(\mathbf{x}_{t_k}^d | \mathbf{h}_{t_k})$. Figure 13 shows that improvements from conditional on both past and concurrent values are robust. The improvement is modest because in this study the hidden state already captures the dependence structure of all variables from the

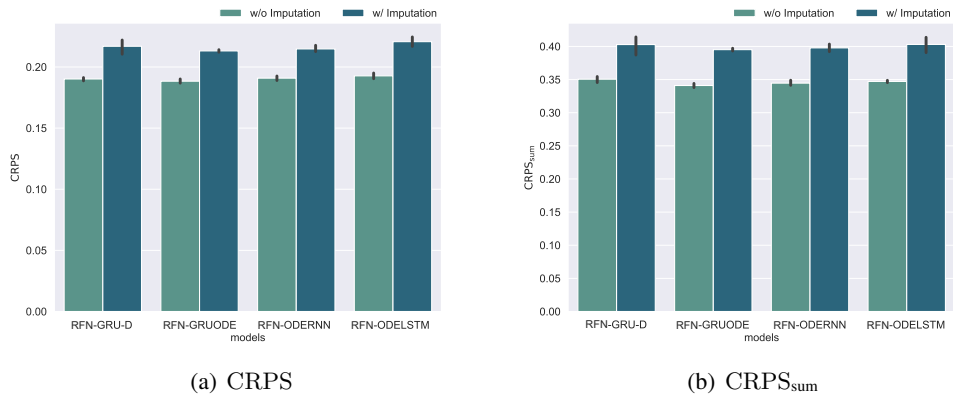


Figure 12: Asynchronous data: Imputing unobserved variables (right bars in darker green) vs Not imputing them (left bars in lighter green).

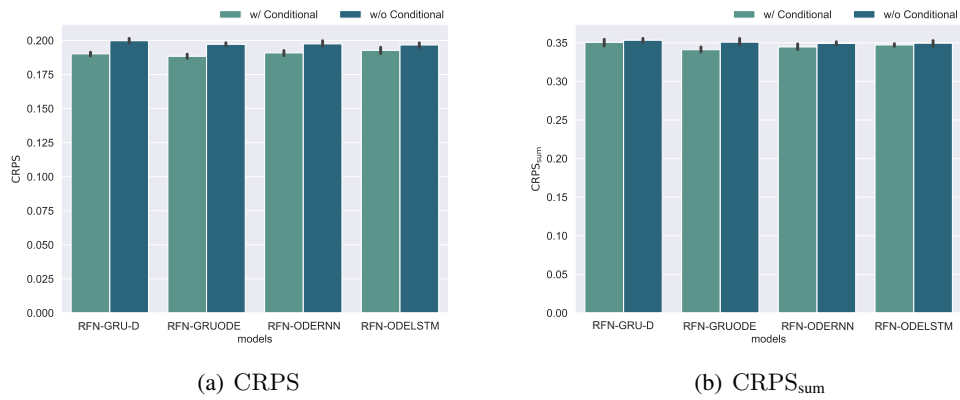


Figure 13: Asyn-MTS model: Using concurrent variables (left bars in lighter green) vs. Without using them (right bars in darker green).

previous time step. In other words, if the dependence structure remains relatively stable at the current time step, the added value of incorporating the new incoming data is incremental.

7.4 Dataset of Physical Activities (MuJoCo)

In applications such as robotics, multivariate time series are commonly used to capture the position, speed, and trajectory of objects, exhibiting a high degree of correlation among variables. It is crucial to understand the dependence structure within these time series. However, irregular and asynchronous frequency of measurements frequently arises due to limitations in measurement devices. This experiment tests the performance of using the RFN specification to predict object positions against baseline models in their vanilla forms.

The MuJoCo physics dataset is first introduced in [17] to verify that the ODE-based models can learn an approximation of Newtonian physics. The dataset is created by the “Hopper” model from the Deepmind Control Suite [45], and it contains 14 variables in total, where the first 7 variables and the last 7 variables control the position and the velocities of the “Hopper”, respectively.

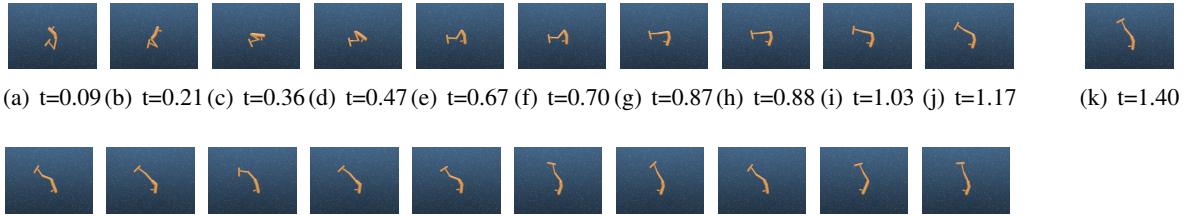


Figure 14: (a)-(j) represent data observed at historical times with unevenly spaced intervals. The objective is to estimate the data distribution at $t=1.40$. Fig. (k) displays the observed ground truth at $t=1.40$. We train the Syn-MTS and Asyn-MTS models to forecast the desired distribution at $t=1.40$. The first and last five figure in the second row displays five samples generated from the trained Syn-MTS model (Asyn-MTS model) at $t=1.40$.

By following the generation and preprocessing of [17], we randomly sample the initial position and velocities of ‘‘Hopper’’ such that the hopper rotates in the air and falls on the ground. We generate 5,000 regularly-sampled time series instances with 150 observed time points for each instance, and randomly sample 50% values to generate the Syn-MTS and Asyn-MTS datasets.

Table 2 shows that the RFNs perform robustly better than the baselines in their vanilla form. As a validation, we use the trained model to forecast the future joint distribution at $t=1.40$ based on a given instance’s past ten observations (ranging from $t=0.09$ to $t=1.17$). Subsequently, we generate 10 samples from the estimated distribution at $t=1.40$ and compare them with the ground truth at $t=1.40$. Figure 14 displays the 10 samples at $t=1.40$ from both the Asyn-MTS model and the Syn-MTS model. They all resemble the ground truth closely, affirming the RFN’s proficiency in predicting the joint distribution.

Table 2: **Physical Activities of Human Body (MuJoCo)**. (Same reporting formats as in Table 1)

model	CRPS	CRPS _{sum}	model	CRPS	CRPS _{sum}	CRPS \uparrow	CRPS _{sum} \uparrow
<i>Syn-MTS</i>							
GRUODE	0.2312 ± 0.0056	1.0877 ± 0.0776	RFN-GRUODE	0.2336 ± 0.0032	1.0570 ± 0.0392	-1.04%	2.82%
ODELSTM	0.2599 ± 0.0021	1.3501 ± 0.0417	RFN-ODELSTM	0.2593 ± 0.0064	1.2163 ± 0.0563	0.24%	9.91%
GRU-D	0.2465 ± 0.0058	1.1992 ± 0.0484	RFN-GRU-D	0.2229 ± 0.0033	1.0140 ± 0.0409	9.58%	15.44%
ODERNN	0.2258 ± 0.0077	1.0571 ± 0.0578	RFN-ODERNN	0.2204 ± 0.0059	0.9929 ± 0.0194	2.37%	6.07%
<i>Asyn-MTS</i>							
GRUODE	0.2950 ± 0.0066	1.1519 ± 0.0212	RFN-GRUODE	0.2183 ± 0.0025	0.8382 ± 0.0099	25.98%	27.24%
ODELSTM	0.3259 ± 0.0088	1.2946 ± 0.0479	RFN-ODELSTM	0.2403 ± 0.0065	0.8911 ± 0.0279	26.26%	31.17%
GRU-D	0.2584 ± 0.0064	1.0170 ± 0.0352	RFN-GRU-D	0.2112 ± 0.0027	0.8155 ± 0.0019	18.27%	19.81%
ODERNN	0.2955 ± 0.0042	1.1476 ± 0.0179	RFN-ODERNN	0.2403 ± 0.0050	0.9060 ± 0.0192	18.67%	21.05%

7.5 Dataset of Climate Records (USHCN)

Variables in natural phenomena, such as climate data, also display strong serial and cross correlations. For instance, temperature values from one season provide valuable information about temperature patterns in the following season. Additionally, precipitation, such as rain and snow, can cause temperature drops and affect humidity levels. Missing observations are also common in climate data due to inclement weather or equipment malfunctions. In this experiment, we evaluate the performance of the RFN specification on the USHCN dataset.

The United States Historical Climatology Network (USHCN) dataset [26] consists of daily measurements from 1,218 centers across the country. It includes 5 variables: precipitation, snowfall, snow depth, maximum

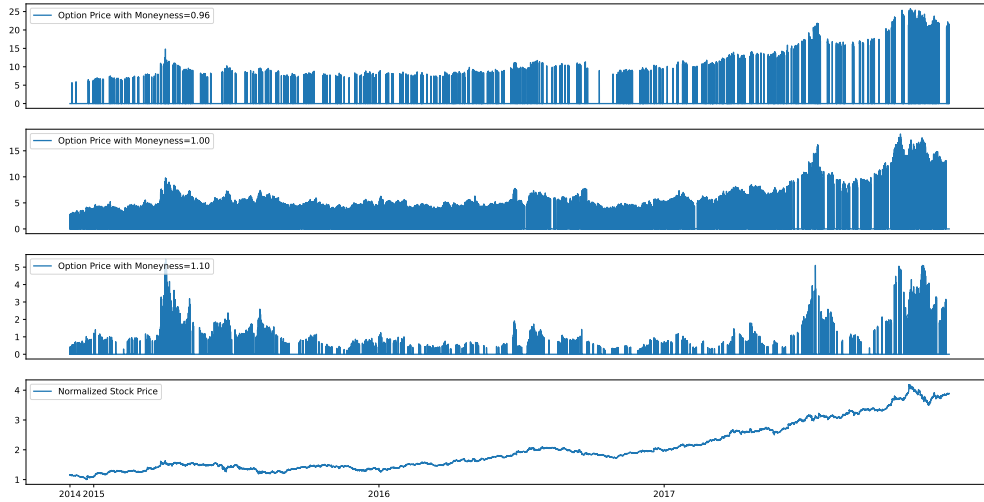


Figure 15: Transaction prices and times of the Tencent stock and its options with moneyness levels 0.96 (in the money), 1.00 (at the money), and 1.10 (out the money) from 01/Dec/2014 to 31/Dec/2017. Values are "missing" means there are no transaction records during the 3-minute intervals.

temperature, and minimum temperature. Following the preprocessing approach of [16], we select the training data from the first quarter of the last four years (1996-2000). This yields 4,494 instances, with each instance’s time period normalized from 0 to 12.5 at intervals of 0.1. The observations for each variable have uneven spacing, making the dataset asynchronous. Consequently, we exclusively employ the Asyn-MTS model for training this dataset.

The results presented in Table 3 demonstrate the superior performance of the RFN specification over its vanilla counterpart for all baselines when applied to the climate dataset. These findings reinforce that climate data does not conform to a multivariate Gaussian distribution and highlight the importance of capturing the dependence structure among variables for accurate weather forecasting.

Table 3: **Climate Records of Weather (USHCN)**. (Same reporting formats as in Table 1)

model	CRPS	CRPS _{sum}	model	CRPS	CRPS _{sum}	CRPS \uparrow	CRPS _{sum} \uparrow
GRUODE	0.3129 ± 0.0024	0.5914 ± 0.0031	RFN-GRUODE	0.2605 ± 0.0153	0.5385 ± 0.0229	16.75%	8.94%
ODELSTM	0.3113 ± 0.0049	0.5909 ± 0.0075	RFN-ODELSTM	0.2723 ± 0.0222	0.5494 ± 0.0264	12.54%	7.02%
GRU-D	0.3048 ± 0.0030	0.5829 ± 0.0066	RFN-GRU-D	0.2636 ± 0.0133	0.5382 ± 0.0179	13.51%	7.66%
ODERNN	0.3124 ± 0.0022	0.5917 ± 0.0039	RFN-ODERNN	0.2544 ± 0.0095	0.5276 ± 0.0139	18.57%	10.84%

7.6 Dataset of Financial Transactions (Stock Options)

Stock options are financial derivatives used for speculation and hedging purposes, allowing investors to buy or sell company stock at a predetermined price (the strike) within a specified time period (the maturity). Models in financial mathematics assume that the underlying stock follows a specific stochastic differential equation, such as the Heston model [46] or the SABR model [47], but require a concurrent set of option prices at different strikes to calibrate the parameters. However, options with different strikes have varying

liquidities in reality, with ATM options trading more frequently than ITM and OTM ones³. This liquidity disparity is illustrated in Figure 15 using the transaction records of Tencent, the stock with the largest market capitalization in the HKEX, and its options with moneyness (defined as the ratio of a strike over by the stock price) of 0.96, 1.00, and 1.10. Figure 15 clearly shows that options with different moneyness do not align, and they are all unevenly spaced. In particular, the ATM option has a higher trading frequency than the ITM and OTM options. It is also evident that the price movements of options are strongly correlated with that of the underlying stock.

We use the Asyn-MTS model to simultaneously forecast the joint distribution of the ATM, OTM, and ITM option prices and the underlying stock price, each of which is considered a unique variable. The dataset is obtained from HKEX, comprising 3-minute level trading records for the stock and its options from 01/Dec/2014 to 31/Dec/2017. We divide the transaction data for each day into one instance, resulting in a total of 720 instances, with each instance having a time length of 110 (where each time step represents 3 minutes, and the trading time for one day is 5.5 hours). We construct 16 variables, where one variable represents the underlying stock price and the other 15 variables represent options with moneyness ranging from 0.96 to 1.10.

Table 4 presents the experiment results, showing that RFNs achieve lower CRPS and CRPS_{sum} compared to the baselines. The predicted quantile intervals for one-day transaction records are visualized in Figure 16. Although options with moneyness 0.96 and 1.10 have no trading, we can also predict their trends by leveraging the cross-sectional information from other options. These results suggest that the RFN specification applies well to option price prediction by capturing the dependence structure between irregularly transacted prices of the underlying stock and its options.

Table 4: **Transaction Records of the Tencent Stock and its Options (HKEX)**. (Same reporting formats as in Table 1)

model	CRPS	CRPS _{sum}	model	CRPS	CRPS _{sum}	CRPS [↑]	CRPS _{sum} [↑]
GRUODE	0.1960 ± 0.0103	0.5645 ± 0.0435	RFN-GRUODE	0.1645 ± 0.0035	0.4221 ± 0.0305	16.05%	25.22%
ODELSTM	0.1947 ± 0.0116	0.5494 ± 0.0463	RFN-ODELSTM	0.1654 ± 0.0074	0.4138 ± 0.0239	15.06%	24.69%
GRU-D	0.2044 ± 0.0081	0.5677 ± 0.0268	RFN-GRU-D	0.1675 ± 0.0101	0.4199 ± 0.0344	18.07%	26.02%
ODERNN	0.1850 ± 0.0161	0.5208 ± 0.0720	RFN-ODERNN	0.1633 ± 0.0041	0.4070 ± 0.0179	11.73%	21.85%

8 Conclusion

Forecasting the joint distribution of multivariate time series with temporal irregularities and heterogeneous dependence structure is challenging. These irregularities can arise due to insufficient observation or inherent randomness in event occurrences. The perspective we take is that we allow the arrival times of observations, which are the core of the temporal irregularities, to play a central role in the model building process.

The proposed RFN framework consists of a marginal learning block and a multivariate learning block. The marginal learning block captures individual serial dependencies by assigning unique hidden states to component variables and updating them based on arrival times of events. This approach acknowledges the intrinsic nature of temporal irregularities in the data and avoids using imputation methods. The multivariate learning block uses a conditional formulation of the Continuous Normalizing Flow model to incorporate the time-varying hidden states learned from the marginal learning block, as well as the concurrent information, into learning the non-parametric distribution. The log-likelihood objective of RFNs fully acknowledges the irregular spacing and asynchronous pattern in the data.

³At-the-money (ATM) options are options whose strikes are equal to the underlying stock price, whereas in-the-money (ITM) and out-of-the-money (OTM) refer to cases where strike prices are below or above the stock price.

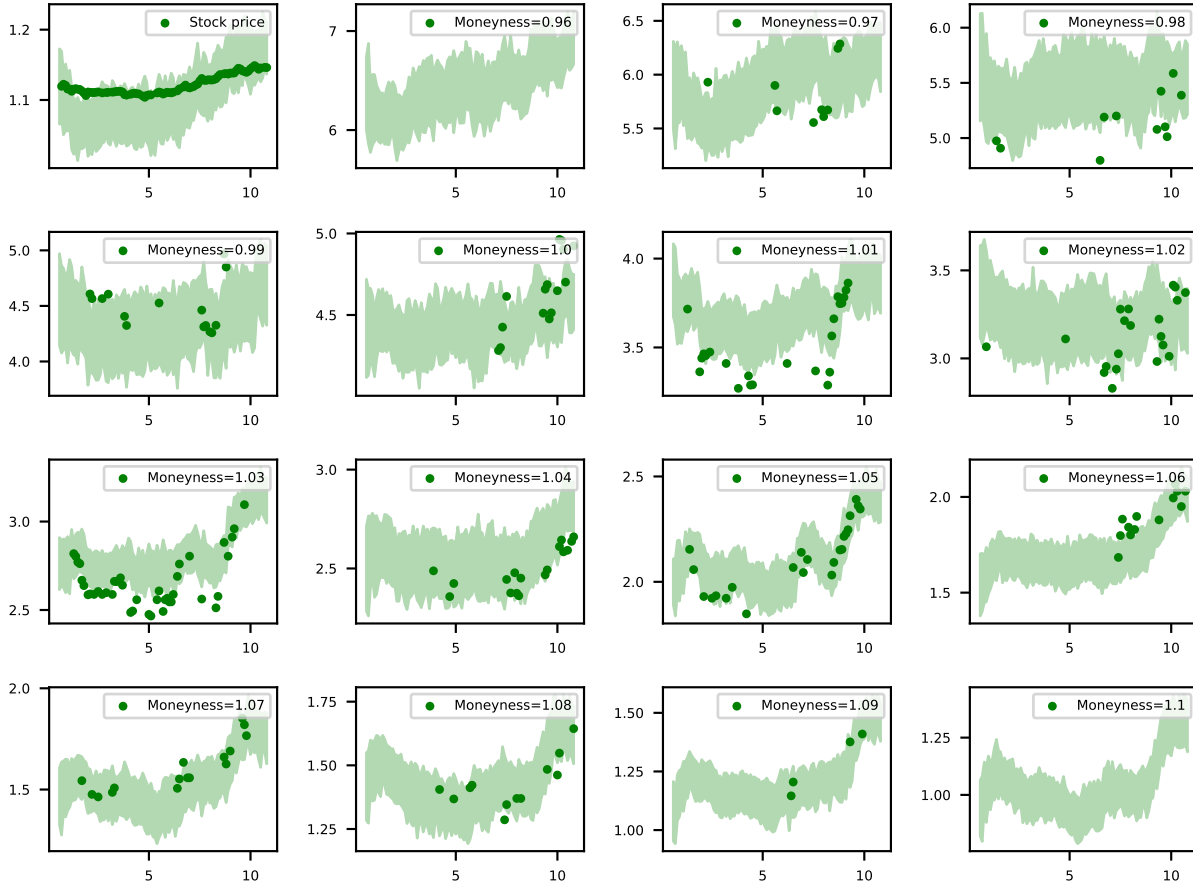


Figure 16: Predicted ranges of quantile (shaded areas)of the Tencent stock price and its options prices. Solid dots represent observed price points.

In the comprehensive evaluations of RFNs using real-world datasets from application domains such as finance, physics, and climate, RFNs consistently outperform models that assume Gaussian distributions for modeling dependence structures in irregularly sampled time series across various state-of-the-art specifications, e.g., GRU-D, GRU-ODE-Bayes, ODELSTM, and ODERNN. These findings highlight the robustness and effectiveness of RFNs.

References

- [1] Hardy Kremer, Stephan Gunnemann, and Thomas Seidl. Detecting climate change in multivariate time series data by novel clustering and cluster tracing techniques. In *2010 IEEE International Conference on Data Mining Workshops*, pages 96–97. IEEE, 2010.
- [2] Gabriel Spadon, Shenda Hong, Bruno Brandoli, Stan Matwin, Jose F Rodrigues-Jr, and Jimeng Sun. Pay attention to evolution: Time series forecasting with deep graph-evolution learning. *IEEE Transactions on Pattern Analysis and Machine Intelligence*, 44(9):5368–5384, 2021.
- [3] Zhiguang Xu, Steven MacEachern, and Xinyi Xu. Modeling non-gaussian time series with nonparametric bayesian model. *IEEE Transactions on Pattern Analysis and Machine Intelligence*, 37(2):372–382,

- 2013.
- [4] Satya Narayan Shukla and Benjamin M Marlin. A survey on principles, models and methods for learning from irregularly sampled time series. *arXiv preprint arXiv:2012.00168*, 2020.
 - [5] Konstantinos Benidis, Syama Sundar Rangapuram, Valentin Flunkert, Yuyang Wang, Danielle Maddix, Caner Turkmen, Jan Gasthaus, Michael Bohlke-Schneider, David Salinas, Lorenzo Stella, et al. Deep learning for time series forecasting: Tutorial and literature survey. *ACM Computing Surveys (CSUR)*, 2018.
 - [6] Gah-Yi Ban, Noureddine El Karoui, and Andrew EB Lim. Machine learning and portfolio optimization. *Management Science*, 64(3):1136–1154, 2018.
 - [7] Yaquan Zhang, Qi Wu, Nanbo Peng, Min Dai, Jing Zhang, and Hu Wang. Memory-gated recurrent networks. In *Proceedings of the AAAI Conference on Artificial Intelligence*, volume 35, pages 10956–10963, 2021.
 - [8] YUAN Zhiri, HU Xixu, WU Qi, MA Shumin, Cheuk Hang Leung, Xin Shen, and Yiyan Huang. A unified domain adaptation framework with distinctive divergence analysis. *Transactions of Machine Learning Research*, 2022.
 - [9] Christopher KI Williams and Carl Edward Rasmussen. *Gaussian processes for machine learning*, volume 2. MIT press Cambridge, MA, 2006.
 - [10] Wei Cao, Dong Wang, Jian Li, Hao Zhou, Lei Li, and Yitan Li. Brits: Bidirectional recurrent imputation for time series. *Advances in neural information processing systems*, 31, 2018.
 - [11] Yonghong Luo, Xiangrui Cai, Ying Zhang, Jun Xu, et al. Multivariate time series imputation with generative adversarial networks. *Advances in neural information processing systems*, 31, 2018.
 - [12] Zhengping Che, Sanjay Purushotham, Kyunghyun Cho, David Sontag, and Yan Liu. Recurrent neural networks for multivariate time series with missing values. *Scientific reports*, 8(1):1–12, 2018.
 - [13] Daniel Neil, Michael Pfeiffer, and Shih-Chii Liu. Phased lstm: Accelerating recurrent network training for long or event-based sequences. *Advances in neural information processing systems*, 29, 2016.
 - [14] Michael C Mozer, Denis Kazakov, and Robert V Lindsey. Discrete event, continuous time rnns. *arXiv preprint arXiv:1710.04110*, 2017.
 - [15] Ricky TQ Chen, Yulia Rubanova, Jesse Bettencourt, and David K Duvenaud. Neural ordinary differential equations. *Advances in neural information processing systems*, 31, 2018.
 - [16] Edward De Brouwer, Jaak Simm, Adam Arany, and Yves Moreau. Gru-ode-bayes: Continuous modeling of sporadically-observed time series. *Advances in neural information processing systems*, 32, 2019.
 - [17] Yulia Rubanova, Ricky TQ Chen, and David K Duvenaud. Latent ordinary differential equations for irregularly-sampled time series. *Advances in neural information processing systems*, 32, 2019.
 - [18] Mathias Lechner and Ramin Hasani. Learning long-term dependencies in irregularly-sampled time series. *arXiv preprint arXiv:2006.04418*, 2020.
 - [19] Junyoung Chung, Kyle Kastner, Laurent Dinh, Kratarth Goel, Aaron C Courville, and Yoshua Bengio. A recurrent latent variable model for sequential data. *Advances in neural information processing systems*, 28, 2015.
 - [20] David Salinas, Valentin Flunkert, Jan Gasthaus, and Tim Januschowski. Deepar: Probabilistic forecasting with autoregressive recurrent networks. *International Journal of Forecasting*, 36(3):1181–1191, 2020.

- [21] David Salinas, Michael Bohlke-Schneider, Laurent Callot, Roberto Medico, and Jan Gasthaus. High-dimensional multivariate forecasting with low-rank gaussian copula processes. *Advances in neural information processing systems*, 32, 2019.
- [22] Ruofeng Wen, Kari Torkkola, Balakrishnan Narayanaswamy, and Dhruv Madeka. A multi-horizon quantile recurrent forecaster. *arXiv preprint arXiv:1711.11053*, 2017.
- [23] Xing Yan, Qi Wu, and Wen Zhang. Cross-sectional learning of extremal dependence among financial assets. *Advances in Neural Information Processing Systems*, 32, 2019.
- [24] Francesco Laio and Stefania Tamea. Verification tools for probabilistic forecasts of continuous hydrological variables. *Hydrology and Earth System Sciences*, 11(4):1267–1277, 2007.
- [25] Kashif Rasul, Abdul-Saboor Sheikh, Ingmar Schuster, Urs Bergmann, and Roland Vollgraf. Multivariate probabilistic time series forecasting via conditioned normalizing flows. *arXiv preprint arXiv:2002.06103*, 2020.
- [26] MJ Menne, CN Williams Jr, and RS Vose. Long-term daily and monthly climate records from stations across the contiguous united states. *Website <http://cdiac.ornl.gov/epubs/ndp/ushcn/access.html> [accessed 23 September 2010]*, 2010.
- [27] Kaiming He, Xiangyu Zhang, Shaoqing Ren, and Jian Sun. Deep residual learning for image recognition. In *Proceedings of the IEEE conference on computer vision and pattern recognition*, pages 770–778, 2016.
- [28] Rupesh Kumar Srivastava, Klaus Greff, and Jürgen Schmidhuber. Highway networks. *arXiv preprint arXiv:1505.00387*, 2015.
- [29] K. Simonyan and A. Zisserman. Very deep convolutional networks for large-scale image recognition. In *International Conference on Learning Representations*, May 2015.
- [30] Christian Szegedy, Wei Liu, Yangqing Jia, Pierre Sermanet, Scott Reed, Dragomir Anguelov, Dumitru Erhan, Vincent Vanhoucke, and Andrew Rabinovich. Going deeper with convolutions. In *Proceedings of the IEEE conference on computer vision and pattern recognition*, pages 1–9, 2015.
- [31] Lev Semenovich Pontryagin. *Mathematical theory of optimal processes*. CRC press, 1987.
- [32] Laurent Dinh, David Krueger, and Yoshua Bengio. Nice: Non-linear independent components estimation. *arXiv preprint arXiv:1410.8516*, 2014.
- [33] Danilo Rezende and Shakir Mohamed. Variational inference with normalizing flows. In *International conference on machine learning*, pages 1530–1538. PMLR, 2015.
- [34] Laurent Dinh, Jascha Sohl-Dickstein, and Samy Bengio. Density estimation using real nvp. *arXiv preprint arXiv:1605.08803*, 2016.
- [35] George Papamakarios, Theo Pavlakou, and Iain Murray. Masked autoregressive flow for density estimation. *Advances in neural information processing systems*, 30, 2017.
- [36] Durk P Kingma and Prafulla Dhariwal. Glow: Generative flow with invertible 1x1 convolutions. *Advances in neural information processing systems*, 31, 2018.
- [37] Ivan Kobyzev, Simon JD Prince, and Marcus A Brubaker. Normalizing flows: An introduction and review of current methods. *IEEE transactions on pattern analysis and machine intelligence*, 43(11): 3964–3979, 2020.
- [38] Will Grathwohl, Ricky TQ Chen, Jesse Bettencourt, Ilya Sutskever, and David Duvenaud. Ffjord: Free-form continuous dynamics for scalable reversible generative models. *arXiv preprint arXiv:1810.01367*, 2018.

- [39] Hrayr Harutyunyan, Hrant Khachatryan, David C Kale, Greg Ver Steeg, and Aram Galstyan. Multitask learning and benchmarking with clinical time series data. *Scientific data*, 6(1):1–18, 2019.
- [40] Francois Belletti, Alex Beutel, Sagar Jain, and Ed Chi. Factorized recurrent neural architectures for longer range dependence. In *international conference on artificial intelligence and statistics*, pages 1522–1530. PMLR, 2018.
- [41] Zhao-Yu Zhang, Shao-Qun Zhang, Yuan Jiang, and Zhi-Hua Zhou. Life: Learning individual features for multivariate time series prediction with missing values. In *2021 IEEE International Conference on Data Mining (ICDM)*, pages 1511–1516. IEEE, 2021.
- [42] James E Matheson and Robert L Winkler. Scoring rules for continuous probability distributions. *Management science*, 22(10):1087–1096, 1976.
- [43] Paul Glasserman. *Monte Carlo methods in financial engineering*, volume 53. Springer, 2004.
- [44] Fischer Black and Myron Scholes. The pricing of options and corporate liabilities. *Journal of political economy*, 81(3):637–654, 1973.
- [45] Yuval Tassa, Yotam Doron, Alistair Muldal, Tom Erez, Yazhe Li, Diego de Las Casas, David Budden, Abbas Abdolmaleki, Josh Merel, Andrew Lefrancq, et al. Deepmind control suite. *arXiv preprint arXiv:1801.00690*, 2018.
- [46] Steven L Heston. A closed-form solution for options with stochastic volatility with applications to bond and currency options. *The review of financial studies*, 6(2):327–343, 1993.
- [47] Patrick S Hagan, Deep Kumar, Andrew S Lesniewski, and Diana E Woodward. Managing smile risk. *The Best of Wilmott*, 1:249–296, 2002.

A Marginal learning blocks

Throughout (A.1),(A.2),(A.3), the operator \odot is the element-wise multiplication and the operator \otimes is defined as in (8).

A.1 GRU-D

GRU-D [12] modifies the classical GRU by adding the trainable exponential decays,

$$\gamma_t = \exp\{-\max(0, \mathbf{w}_\gamma \delta_t + \mathbf{b}_\gamma)\},$$

where δ_t is the time intervals between two observations, and \mathbf{w}_γ and \mathbf{b}_γ are trainable parameters. First, it imputes the missing values with the weighted average between the last observations and the empirical means,

$$\hat{x}_t^d = m_t^d x_t^d + (1 - m_t^d) \left(\gamma_{x_t}^d x_{t'}^d + (1 - \gamma_{x_t}^d) \tilde{x}^d \right),$$

where m_t^d is the mask of d^{th} variable at time t , $\gamma_{x_t}^d$ is the trainable decay, $x_{t'}^d$ is the previous observation ($t' < t$), and \tilde{x}^d is its empirical mean. Second, it employs hidden state decay to further capture the missing patterns in the hidden state,

$$\hat{\mathbf{h}}_{t-1} = \gamma_{h_t} \odot \mathbf{h}_{t-1}.$$

Applying the marginal learning idea to GRU-D, the updating equations are as follows

$$\begin{aligned} \mathbf{r}_t &= \sigma \left(\mathcal{W}_r \otimes \hat{\mathbf{x}}_t + \mathcal{U}_r \otimes \hat{\mathbf{h}}_{t-1} + \mathcal{V}_r \otimes \mathbf{m}_t + \mathbf{b}_r \right), \\ \mathbf{z}_t &= \sigma \left(\mathcal{W}_z \otimes \hat{\mathbf{x}}_t + \mathcal{U}_z \otimes \hat{\mathbf{h}}_{t-1} + \mathcal{V}_z \otimes \mathbf{m}_t + \mathbf{b}_z \right), \\ \tilde{\mathbf{h}}_t &= \tanh \left(\mathcal{W}_h \otimes \hat{\mathbf{x}}_t + \mathcal{U}_h \otimes (\mathbf{r}_t \odot \hat{\mathbf{h}}_{t-1}) + \mathcal{V}_h \otimes \mathbf{m}_t + \mathbf{b}_h \right), \\ \mathbf{h}_t &= \mathbf{z}_t \odot \mathbf{h}_{t-1} + (1 - \mathbf{z}_t) \odot \tilde{\mathbf{h}}_t, \end{aligned}$$

where $\mathcal{W}_{\{r,z,h\}}, \mathcal{U}_{\{r,z,h\}}, \mathcal{V}_{\{r,z,h\}}, \mathbf{b}_{\{r,z,h\}}$ are parameters to be trained,

$$\begin{aligned} \mathcal{W}_{\{r,z,h\}} &= \{\mathbf{w}_{\{r,z,h\}}^1; \dots; \mathbf{w}_{\{r,z,h\}}^D\} \in \mathbb{R}^{D \times S \times 1}, \\ \mathcal{U}_{\{r,z,h\}} &= \{\mathbf{u}_{\{r,z,h\}}^1; \dots; \mathbf{u}_{\{r,z,h\}}^D\} \in \mathbb{R}^{D \times S \times S}, \\ \mathcal{V}_{\{r,z,h\}} &= \{\mathbf{v}_{\{r,z,h\}}^1; \dots; \mathbf{v}_{\{r,z,h\}}^D\} \in \mathbb{R}^{D \times S \times 1}. \end{aligned}$$

A.2 ODERNN

ODERNN [17] proposes handling irregularly sampled time series by modeling the hidden state evolution using a Neural ODE in the absence of observations. Compared to GRU-ODE-Bayes [16], such a Neural ODE does not admit explicit solutions; instead, it is modeled using a standard MLP network. When there are observations, a classical GRU cell will update the hidden state.

When implementing ODERNN to learn the marginal block, we assign each variable with unique training parameters, and thus the evolution formula of ODERNN in the marginal learning block is

$$\frac{d\mathbf{h}^d(t)}{dt} = \mathbf{f}_\theta^d(\mathbf{h}^d(t), t).$$

Let $\mathbf{h}_{t_-} = \mathbf{h}(t_-)$ and $\mathbf{h}_{t_+} = \mathbf{h}(t_+)$, the updating equations of ODERNN for the marginal learning are

$$\begin{aligned} \mathbf{r}_{t_-} &= \sigma(\mathcal{W}_r \otimes \mathbf{x}_t + \mathcal{U}_r \otimes \mathbf{h}_{t_-} + \mathbf{b}_r), \\ \mathbf{z}_{t_-} &= \sigma(\mathcal{W}_z \otimes \mathbf{x}_t + \mathcal{U}_z \otimes \mathbf{h}_{t_-} + \mathbf{b}_z), \\ \tilde{\mathbf{h}}_{t_-} &= \tanh(\mathcal{W}_h \otimes \mathbf{x}_t + \mathcal{U}_h \otimes (\mathbf{r}_t \odot \mathbf{h}_{t_-}) + \mathbf{b}_h), \\ \mathbf{h}_{t_+} &= \mathbf{z}_t \odot \mathbf{h}_{t_-} + (1 - \mathbf{z}_t) \odot \tilde{\mathbf{h}}_{t_-}, \end{aligned}$$

where $\mathcal{W}_{\{r,z,h\}}, \mathcal{U}_{\{r,z,h\}}, \mathbf{b}_{\{r,z,h\}}$ are the trainable parameters,

$$\begin{aligned} \mathcal{W}_{\{r,z,h\}} &= \{\mathbf{w}_{\{r,z,h\}}^1; \dots; \mathbf{w}_{\{r,z,h\}}^D\} \in \mathbb{R}^{D \times S \times 1}, \\ \mathcal{U}_{\{r,z,h\}} &= \{\mathbf{u}_{\{r,z,h\}}^1; \dots; \mathbf{u}_{\{r,z,h\}}^D\} \in \mathbb{R}^{D \times S \times S}. \end{aligned}$$

A.3 ODELSTM

ODELSTM [18] is designed to learn the long-term dependencies in irregularly sampled time series. In the absence of observations, the hidden states are evolved by a Neural ODE, and when there is an observation, the hidden state is updated by the classical LSTM. Unlike the ODERNN and GRU-ODE-Bayes, the cell state of LSTM will contain long-term memory. To cast the ODELSTM in the RFN framework, we assign each variable a unique set of training parameters. It has the following evolution equation

$$\frac{d\mathbf{h}^d(t)}{dt} = \mathbf{f}_\theta^d(\mathbf{h}^d(t), t).$$

Let $\mathbf{h}_{t_-} = \mathbf{h}(t_-)$ and $\mathbf{h}_{t_+} = \mathbf{h}(t_+)$. The updating equations of ODELSTM for the marginal learning are

$$\begin{aligned} \mathbf{f}_{t_-} &= \sigma(\mathcal{W}_f \otimes \mathbf{x}_t + \mathcal{U}_f \otimes \mathbf{h}_{t_-} + \mathbf{b}_f), \\ \mathbf{i}_{t_-} &= \sigma(\mathcal{W}_i \otimes \mathbf{x}_t + \mathcal{U}_i \otimes \mathbf{h}_{t_-} + \mathbf{b}_i), \\ \mathbf{o}_{t_-} &= \sigma(\mathcal{W}_o \otimes \mathbf{x}_t + \mathcal{U}_o \otimes \mathbf{h}_{t_-} + \mathbf{b}_o), \\ \tilde{\mathbf{c}}_{t_-} &= \tanh(\mathcal{W}_c \otimes \mathbf{x}_t + \mathcal{U}_c \otimes \mathbf{h}_{t_-} + \mathbf{b}_c), \\ \mathbf{c}_{t_+} &= \mathbf{f}_{t_-} \odot \mathbf{c}_{(t-1)_+} + \mathbf{i}_{t_-} \odot \tilde{\mathbf{c}}_{t_-} \\ \mathbf{h}_{t_+} &= \mathbf{o}_{t_-} \odot \tanh(\mathbf{c}_{t_+}), \end{aligned}$$

where $\mathcal{W}_{\{f,i,o,c\}}, \mathcal{U}_{\{f,i,o,c\}}, \mathbf{b}_{\{f,i,o,c\}}$ are the parameters to be trained,

$$\begin{aligned} \mathcal{W}_{\{f,i,o,c\}} &= \{\mathbf{w}_{\{f,i,o,c\}}^1; \dots; \mathbf{w}_{\{f,i,o,c\}}^D\} \in \mathbb{R}^{D \times S \times 1}, \\ \mathcal{U}_{\{f,i,o,c\}} &= \{\mathbf{u}_{\{f,i,o,c\}}^1; \dots; \mathbf{u}_{\{f,i,o,c\}}^D\} \in \mathbb{R}^{D \times S \times S}. \end{aligned}$$

B Proof of Lemma 5.1

Proof. Consider the random variables $\mathbf{X} \in \mathbb{R}^D$ and $\mathbf{Y} \in \mathbb{R}^C$. Let $\tilde{\mathbf{Z}}(s) = [\mathbf{Z}(s), \mathbf{Y}(s)]^T$ be a finite continuous random variable. Let the realizations of $\tilde{\mathbf{Z}}(s)$ be $\tilde{\mathbf{z}}(s) = [\mathbf{z}(s), \mathbf{y}(s)]^T$, and the probability density of $\tilde{\mathbf{Z}}(s)$ be $p(\tilde{\mathbf{z}}(s)) = p(\mathbf{z}(s), \mathbf{y}(s))$ which depends on the flow time s , where $s_0 \leq s \leq s_1$. We assume $\mathbf{z}(s)$ evolves continuously in the real space, starting from a sample point of a pre-defined distribution at $s = s_0$ and ending at a sample point \mathbf{x} of \mathbf{X} at $s = s_1$. According to (5a), the governing equation of $\tilde{\mathbf{z}}(s)$ can be written as

$$\frac{\partial \tilde{\mathbf{z}}(s)}{\partial s} = \begin{bmatrix} \frac{\partial \mathbf{z}(s)}{\partial s} \\ \frac{\partial \mathbf{y}(s)}{\partial s} \end{bmatrix} = \begin{bmatrix} \mathbf{f}(\mathbf{z}(s), s, \mathbf{y}(s); \theta) \\ 0 \end{bmatrix}, \text{ where } s_0 \leq s \leq s_1,$$

$y(s) = y$ and $z(s_1) = x$. From the differential equation $\frac{\partial y(s)}{\partial s} = 0$, we have $y(s) = y$. Hence, we are going to find the density $p(\tilde{z}_s) = p(z_s, y)$ such that

$$\frac{\partial z(s)}{\partial s} = f(z(s), s, y; \theta).$$

The proof requires the change of variables in the probability density theorem. We restate the result below.

Result. *Suppose that $G(\cdot)$ is a bijective function and differentiable. Given the variables (Z, Y) and the corresponding density function $p(z, y)$, the density function of $(G(Z), Y)$ is*

$$\begin{aligned} p(G(z), y) &= p(z, y) \left| \det \begin{bmatrix} \partial_z G(z) & 0_{D \times C} \\ 0_{C \times D} & \mathbb{I}_C \end{bmatrix} \right|^{-1} \\ \Rightarrow \log p(G(z), y) &= \log p(z, y) - \log \left| \det \begin{bmatrix} \partial_z G(z) & 0_{D \times C} \\ 0_{C \times D} & \mathbb{I}_C \end{bmatrix} \right|. \end{aligned} \quad (25)$$

Now, we consider $\frac{\partial \log p(\tilde{z}(s))}{\partial s} = \frac{\partial \log p(z(s), y)}{\partial s}$. We write $\tilde{z}(s + \epsilon) = [z(s + \epsilon), Y]' = [T_\epsilon(z(s)), Y]'$. From the first principle of derivatives, we have

$$\begin{aligned} \partial_s \log p(\tilde{z}(s)) &= \lim_{\epsilon \rightarrow 0^+} \frac{\log p(\tilde{z}(s + \epsilon)) - \log p(\tilde{z}(s))}{\epsilon} \\ &= \lim_{\epsilon \rightarrow 0^+} \frac{\log p(T_\epsilon(z(s)), y) - \log p(z(s), y)}{\epsilon}. \end{aligned}$$

We simplify the quantity $\lim_{\epsilon \rightarrow 0^+} \frac{\log p(T_\epsilon(z(s)), y) - \log p(z(s), y)}{\epsilon}$. Applying equation (25), we have

$$\begin{aligned} \partial_s \log p(\tilde{z}(s)) &= \lim_{\epsilon \rightarrow 0^+} \frac{-\log \left| \det \begin{bmatrix} \partial_{z(s)} T_\epsilon(z(s)) & 0_{D \times C} \\ 0_{C \times D} & \mathbb{I}_C \end{bmatrix} \right|}{\epsilon} \\ &\stackrel{\text{L'Hôpital}}{=} - \lim_{\epsilon \rightarrow 0^+} \partial_\epsilon \log \left| \det \begin{bmatrix} \partial_{z(s)} T_\epsilon(z(s)) & 0_{D \times C} \\ 0_{C \times D} & \mathbb{I}_C \end{bmatrix} \right| = - \lim_{\epsilon \rightarrow 0^+} \frac{\partial_\epsilon \left| \det \begin{bmatrix} \partial_{z(s)} T_\epsilon(z(s)) & 0_{D \times C} \\ 0_{C \times D} & \mathbb{I}_C \end{bmatrix} \right|}{\left| \det \begin{bmatrix} \partial_{z(s)} T_\epsilon(z(s)) & 0_{D \times C} \\ 0_{C \times D} & \mathbb{I}_C \end{bmatrix} \right|} \\ &= \frac{- \lim_{\epsilon \rightarrow 0^+} \partial_\epsilon \left| \det \begin{bmatrix} \partial_{z(s)} T_\epsilon(z(s)) & 0_{D \times C} \\ 0_{C \times D} & \mathbb{I}_C \end{bmatrix} \right|}{\underbrace{\lim_{\epsilon \rightarrow 0^+} \left| \det \begin{bmatrix} \partial_{z(s)} T_\epsilon(z(s)) & 0_{D \times C} \\ 0_{C \times D} & \mathbb{I}_C \end{bmatrix} \right|}_1} = - \lim_{\epsilon \rightarrow 0^+} \partial_\epsilon \left| \det \begin{bmatrix} \partial_{z(s)} T_\epsilon(z(s)) & 0_{D \times C} \\ 0_{C \times D} & \mathbb{I}_C \end{bmatrix} \right|. \end{aligned}$$

Applying the Jacobi's formula, we have

$$\begin{aligned} \partial_s \log p(\tilde{z}(s)) &= - \lim_{\epsilon \rightarrow 0^+} \text{Tr} \left(\text{adj} \left(\begin{bmatrix} \partial_{z(s)} T_\epsilon(z(s)) & 0_{D \times C} \\ 0_{C \times D} & \mathbb{I}_C \end{bmatrix} \right) \times \partial_\epsilon \begin{bmatrix} \partial_{z(s)} T_\epsilon(z(s)) & 0_{D \times C} \\ 0_{C \times D} & \mathbb{I}_C \end{bmatrix} \right) \\ &= - \text{Tr} \left(\underbrace{\lim_{\epsilon \rightarrow 0^+} \text{adj} \left(\begin{bmatrix} \partial_{z(s)} T_\epsilon(z(s)) & 0_{D \times C} \\ 0_{C \times D} & \mathbb{I}_C \end{bmatrix} \right)}_{\mathbb{I}_C} \times \lim_{\epsilon \rightarrow 0^+} \frac{\partial}{\partial \epsilon} \begin{bmatrix} \partial_{z(s)} T_\epsilon(z(s)) & 0_{D \times C} \\ 0_{C \times D} & \mathbb{I}_C \end{bmatrix} \right) \\ &= - \text{Tr} \left(\lim_{\epsilon \rightarrow 0^+} \left(\partial_\epsilon \partial_{z(s)} T_\epsilon(z(s)) \right) \right). \end{aligned}$$

Applying Taylor series expansion on $T_\epsilon(\mathbf{z}(s))$ and taking the limit, we have

$$\begin{aligned}
 \partial_s \log p(\tilde{\mathbf{z}}(s)) &= -\text{Tr} \left(\lim_{\epsilon \rightarrow 0^+} \left(\partial_\epsilon \partial_{\mathbf{z}(s)} T_\epsilon(\mathbf{z}(s)) \right) \right) \\
 &= -\text{Tr} \left(\lim_{\epsilon \rightarrow 0^+} \left(\partial_\epsilon \partial_{\mathbf{z}(s)} (\mathbf{z}(s) + \partial_s \mathbf{z}(s) \epsilon + O(\epsilon^2)) \right) \right) \\
 &= -\text{Tr} \left(\lim_{\epsilon \rightarrow 0^+} \left(\partial_\epsilon (\mathbb{I} + \partial_{\mathbf{z}(s)} f(\mathbf{z}(s), s, \mathbf{y}; \theta)) \epsilon + O(\epsilon^2) \right) \right) \\
 &= -\text{Tr} \left(\partial_{\mathbf{z}(s)} f(\mathbf{z}(s), s, \mathbf{y}; \theta) \right).
 \end{aligned}$$

As such, we have

$$\begin{aligned}
 \int_{s_0}^{s_1} \partial_s \log p(\tilde{\mathbf{z}}(s)) ds &= \int_{s_0}^{s_1} -\text{Tr} \left(\partial_{\mathbf{z}(s)} f(\mathbf{z}(s), s, \mathbf{y}; \theta) \right) ds \\
 \Rightarrow \log p(\tilde{\mathbf{z}}(s_1)) &= \log p(\tilde{\mathbf{z}}(s_0)) + \int_{s_1}^{s_0} \text{Tr} \left(\partial_{\mathbf{z}(s)} f(\mathbf{z}(s), s, \mathbf{y}; \theta) \right) ds \\
 \Rightarrow \log p(\mathbf{z}(s_1), \mathbf{y}) &= \log p(\mathbf{z}(s_0), \mathbf{y}) + \int_{s_1}^{s_0} \text{Tr} \left(\partial_{\mathbf{z}(s)} f(\mathbf{z}(s), s, \mathbf{y}; \theta) \right) ds.
 \end{aligned}$$

□

C More Experiment Results

In section 7.3 (c) Data and Model Validation, the prediction intervals of Figure 9 are restricted to quantiles ranging from 0.2 to 0.8. Here, we present results with a broader quantile range in Figure 17.

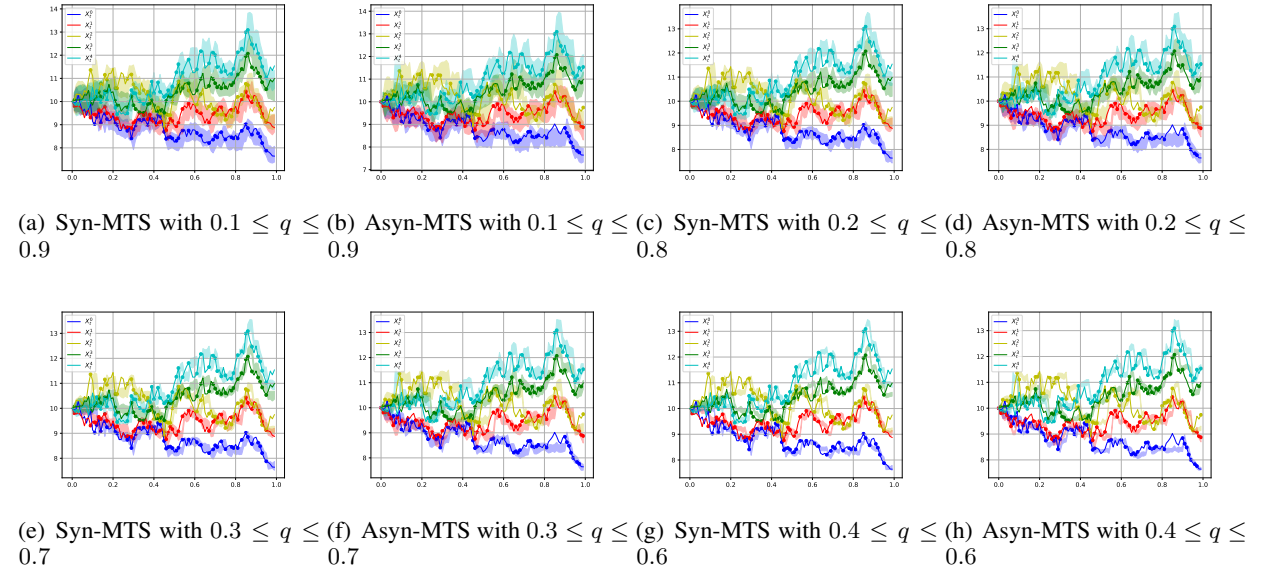


Figure 17: Predicted ranges of quantile (shaded areas) of the simulated Syn-MTS and Asyn-MTS at various probability intervals q .

D Algorithms of Training and Sampling of Syn-MTS and Asyn-MTS

The training process should proceed sequentially to compute the hidden state and the joint distribution of all variables at each observed time point.

For example, in a Syn-MTS instance with two variables observed at time points t_1, t_3, t_5 , we first compute the hidden state \mathbf{h}_{t_1-} and feed the observation \mathbf{x}_{t_1} into the flow model f_θ to obtain the joint distribution at t_1 . Then, we evolve the hidden states to t_3 and feed the observation \mathbf{x}_{t_3} into the flow model f_θ to obtain the joint distribution at t_3 , and so on so force. However, this process is time-consuming since we must call the flow model t_K times.

To reduce the complexity, we first evolve the hidden states to the final time point and store all the necessary parameters at each time point. For example, we compute and store the base distribution parameters at each time point, e.g., $\{\mu_{t_1}, \Sigma_{t_1}\} = \mathbf{MLP}(\mathbf{h}_{t_1-}; \psi)$, $\{\mu_{t_3}, \Sigma_{t_3}\} = \mathbf{MLP}(\mathbf{h}_{t_3-}; \psi)$, and $\{\mu_{t_5}, \Sigma_{t_5}\} = \mathbf{MLP}(\mathbf{h}_{t_5-}; \psi)$. We then concatenate all the observations and the stored parameters together, i.e., $\mathbf{x}_t = \{\mathbf{x}_{t_1}, \mathbf{x}_{t_3}, \mathbf{x}_{t_5}\}$, $\mu_t = \{\mu_{t_1}, \mu_{t_3}, \mu_{t_5}\}$, $\Sigma_t = \{\Sigma_{t_1}, \Sigma_{t_3}, \Sigma_{t_5}\}$. Finally, we feed \mathbf{x}_t to the flow model f_θ to transform the values at all time points simultaneously. This approach requires only one call to the flow model.

Algorithm 1 Algorithm for training and sampling process of Syn-MTS (example of RFN-GRUODE)

```

1: Training (Syn-MTS):
2: Input: Observations:  $\{\mathbf{x}_i\}_{i=1}^N$ ; Masks:  $\{\mathbf{m}_i\}_{i=1}^N$ ; Observed time points:  $\{t_i = [t_1, \dots, t_{K_i}]\}_{i=1}^N$ ; Flow time interval  $[s_1, s_0]$ 
3: Initialize: time = 0,  $\mathbf{h}_0$ , and all trainable parameters  $\zeta^c, \zeta^u, \psi, \theta$ 
4: for  $i = 1$  to  $N$  do
5:   for  $k = 1$  to  $K_i$  do
6:      $\mathbf{h}(t_{k-}) = \text{Continuous Updating}(\mathbf{h}(t_{(k-1)+}), \text{time}, t_k; \zeta^c)$  % marginal hidden state evolves to  $t_k$ 
7:      $\mu_{t_k}, \Sigma_{t_k} = \mathbf{MLP}(\mathbf{h}_{t_{k-}}; \psi)$  % predict and store the parameters of base distribution at  $t_k$ 
8:     time =  $t_k$ 
9:      $\mathbf{h}(t_{k+}) = \text{Discrete Updating}(\mathbf{h}(t_{k-}), \mathbf{x}_{t_k}, \mathbf{m}_{t_k}; \zeta^u)$  % marginal memory updates at  $t_k$ 
10:   end for
11:   % concatenate observations and parameters at all time points and transform them at the same time by the flow model
12:   Set  $t \in \{t_1^i, \dots, t_{K_i}^i : \mathbf{m}_{t_k} = 1, k \in \{1, \dots, K_i\}\}$  % all the observed time points
13:    $\mathbf{z}_t = \mathbf{x}_t + \int_{s_1}^{s_0} \mathbf{f}(\mathbf{z}(s), s, \mathbf{h}_{t-}; \theta) ds$  % transform observations from data distribution to base distribution (from  $s_1$  to  $s_0$ )
14:    $\log p(\mathbf{z}_t | \mathbf{h}_{t-}) = \log p(\mathbf{z}_t; \mu_t, \Sigma_t)$  % compute the log-likelihood of transformed observations in base distribution
15:    $\log p(\mathbf{x}_t | \mathbf{h}_{t-}) = \log p(\mathbf{z}_t | \mathbf{h}_{t-}) + \int_{s_1}^{s_0} \text{Tr}[\partial_{\mathbf{z}(s)} \mathbf{f}] ds$  % compute the log-likelihood of observed data points
16:    $\mathcal{L}_{\text{Syn-MTS}}^i = -\log p(\mathbf{x}_t | \mathbf{h}_{t-})$  % compute the loss of sample  $i$  by equation (17)
17: end for
18:  $\mathcal{L}_{\text{Syn-MTS}} = \frac{1}{N} \sum_{i=1}^N \mathcal{L}_{\text{Syn-MTS}}^i$  % compute the total loss by averaging the loss of all the samples
19:  $\zeta^c, \zeta^u, \psi, \theta \leftarrow \arg \min_{\zeta^c, \zeta^u, \psi, \theta} \mathcal{L}_{\text{Syn-MTS}}$  % optimize the training parameters via stochastic gradient descent algorithm
20:
21: Sampling (Syn-MTS):
22: Input: Observations  $\mathbf{x}_i$ ; Masks  $\mathbf{m}_i$ ; Observed time points  $t_i = [t_1, \dots, t_{K_i}]$ ; Flow time interval  $[s_0, s_1]$ ; Trained model  $\mathbf{f}$ 
23: Initialize: time = 0,  $\mathbf{h}_0$ 
24: for  $k = 1$  to  $K_i$  do
25:    $\mathbf{h}(t_{k-}) = \text{Continuous Updating}(\mathbf{h}(t_{(k-1)+}), \text{time}, t_k)$  % marginal hidden state evolves to  $t_k$ 
26:    $\mu_{t_k}, \Sigma_{t_k} = \mathbf{MLP}(\mathbf{h}_{t_{k-}}; \psi)$  % predict the parameters of base distribution at  $t_k$ 
27:    $\mathbf{z}_{t_k} \sim N(\mu_{t_k}, \Sigma_{t_k})$  % sampling samples in predicted base distribution
28:    $\mathbf{x}_{t_k} = \mathbf{z}_{t_k} + \int_{s_0}^{s_1} \mathbf{f}(\mathbf{z}(s), s, \mathbf{h}_{t_{k-}}; \theta) ds$  % transform the samples from base distribution to data distribution (from  $s_0$  to  $s_1$ )
29:   time =  $t_k$ 
30:    $\mathbf{h}(t_{k+}) = \text{Discrete Updating}(\mathbf{h}(t_{k-}), \mathbf{x}_{t_k}, \mathbf{m}_{t_k})$  % marginal memory updates at  $t_k$ 
31: end for
32: return  $\mathbf{x}_t$ 

```

Algorithm 2 Algorithm for training and sampling process of Asyn-MTS (example of RFN-GRUODE)

```

1: Training (Asyn-MTS):
2: Input: Observations:  $\{\mathbf{x}_i\}_{i=1}^N$ ; Masks:  $\{\mathbf{m}_i\}_{i=1}^N$ ; Observed time points:  $\{t_i = [t_1, \dots, t_{K_i}]\}_{i=1}^N$ ; Flow time interval  $[s_1, s_0]$ 
3: Initialize: time = 0,  $\mathbf{h}_0$ , and all trainable parameters  $\zeta^c, \zeta^u, \psi_m, \theta, \eta$ 
4: for  $i = 1$  to  $N$  do
5:   for  $k = 1$  to  $K_i$  do
6:      $\mathbf{h}(t_{k-}) = \text{Continuous Updating}(\mathbf{h}(t_{(k-1)+}), \text{time}, t_k; \zeta^c)$  % marginal hidden state evolves to  $t_k$ 
7:      $\mu_{t_k}^d, \Sigma_{t_k}^d = \mathbf{m}\text{-MLP}(\mathbf{h}_{t_{k-}}, \mathbf{x}_{t_k}^{-d}; \psi_m)$  % predict the parameters of base distribution at  $t_k$ ,  $\mu$  and  $\Sigma$  are masked-MLPs
8:      $\tilde{\mathbf{x}}_{t_k} = g(\mathbf{h}_{t_{k-}}; \eta)$  % predict the values of variables at  $t_k$ 
9:      $\tilde{\mathbf{x}}_{t_k} = \mathbf{x}_{t_k} \odot \mathbf{m}_{t_k} + \tilde{\mathbf{x}}_{t_k} \odot (1 - \mathbf{m}_{t_k})$  % impute the variables that are unobserved at  $t_k$ 
10:    time =  $t_k$ 
11:     $\mathbf{h}(t_{k+}) = \text{Discrete Updating}(\mathbf{h}(t_{k-}), \mathbf{x}_{t_k}, \mathbf{m}_{t_k}; \zeta^u)$  % marginal memory updates at  $t_k$ 
12:  end for
13:  % concatenate observations and parameters at all time points and transform them at the same time by the flow model
14:  for  $d = 1$  to  $D$  do
15:    Set  $t \in \{t_1^d, \dots, t_{K_i}^d : m_{t_k}^d = 1, k \in \{1, \dots, K_i\}\}$  % all the observed time points for variable  $d$ 
16:     $z_t^d = x_t^d + \int_{s_1}^{s_0} \mathbf{f}(z^d(s), s, \mathbf{h}_{t_{k-}}, \tilde{\mathbf{x}}_{t_k}^{-d}; \theta) ds$  % transform data distribution of observed variable  $d$  to base distribution
17:     $\log p(z_t^d | \mathbf{h}_{t_{k-}}, \tilde{\mathbf{x}}_{t_k}^{-d}) = \log p(z_t^d; \mu_t^d, \Sigma_t^d)$  % compute the log-likelihood of observations of variable  $d$  in base distribu-
tion
18:     $\log p(x_t^d | \mathbf{h}_{t_{k-}}, \tilde{\mathbf{x}}_{t_k}^{-d}) = \log p(z_t^d | \mathbf{h}_{t_{k-}}, \tilde{\mathbf{x}}_{t_k}^{-d}) + \int_{s_1}^{s_0} \text{Tr}[\partial_{z^d(s)} \mathbf{f}] ds$  % compute the log-likelihood of observed data
points
19:     $\mathcal{L}_{\text{Asyn-MTS}}^{d,i} = -\log p(x_t^d | \mathbf{h}_{t_{k-}}, \tilde{\mathbf{x}}_{t_k}^{-d})$  % only compute the negative log-likelihood loss for the observed variables
20:     $\mathcal{L}_{\text{MSE}}^{d,i} = (x_t^d - \hat{x}_t^d)^2$  % compute the MSE loss for imputation
21:  end for
22:   $\mathcal{L}_{\text{Asyn-MTS}}^i = \sum_{d=1}^D (\mathcal{L}_{\text{Asyn-MTS}}^{d,i} + \mathcal{L}_{\text{MSE}}^{d,i})$  % compute the loss of sample  $i$  by equation (22)
23: end for
24:  $\mathcal{L}_{\text{Asyn-MTS}} = \frac{1}{N} \sum_{i=1}^N \mathcal{L}_{\text{Asyn-MTS}}^i$  % compute the total loss by averaging the loss of all the samples
25:  $\zeta^c, \zeta^u, \psi_m, \theta, \eta \leftarrow \arg \min_{\zeta^c, \zeta^u, \psi_m, \theta, \eta} \mathcal{L}_{\text{Asyn-MTS}}$  % optimize the training parameters via stochastic gradient descent algorithm
26:
27: Sampling (Asyn-MTS):
28: Input: Observations:  $\mathbf{x}_i$ ; Masks:  $\mathbf{m}_i$ ; Observed time points:  $t_i = [t_1, \dots, t_{K_i}]$ ; Flow time interval  $[s_0, s_1]$ ; Trained model  $\mathbf{f}$ 
29: Initialize: time = 0,  $\mathbf{h}_0$ 
30: for  $k = 1$  to  $K_i$  do
31:    $\mathbf{h}(t_{k-}) = \text{Continuous Updating}(\mathbf{h}(t_{(k-1)+}), \text{time}, t_k; \zeta^c)$  % marginal hidden state evolves to  $t_k$ 
32:   for  $d = 1$  to  $D$  do
33:      $\mu_{t_k}^d, \Sigma_{t_k}^d = \mathbf{m}\text{-MLP}(\mathbf{h}_{t_{k-}}, \mathbf{x}_{t_k}^{-d})$  % predict the parameters of base distribution for variable  $d$  at  $t_k$ 
34:      $z_{t_k}^d \sim N(\mu_{t_k}^d, \Sigma_{t_k}^d)$  % sampling samples in predicted base distribution
35:      $x_{t_k}^d = z_{t_k}^d + \int_{s_0}^{s_1} \mathbf{f}(z^d(s), s, \mathbf{h}_{t_{k-}}, \mathbf{x}_{t_k}^{-d}; \theta) ds$  % transform the samples from base distributions to data distributions
36:   end for
37:   time =  $t_k$ 
38:    $\mathbf{h}(t_{k+}) = \text{Discrete Updating}(\mathbf{h}(t_{k-}), \mathbf{x}_{t_k}, \mathbf{m}_{t_k}; \zeta^u)$  % marginal memory updates at  $t_k$ 
39: end for
40: return  $\mathbf{x}_t$ 

```